الجمهورية الجزائرية الديمقراطية الشعبية

People's Democratic Republic of Algeria

وزارة التعليم العالي و البحث العلمي

Ministry Of Higher Education And Scientific Research

جامعة الشهيد حمه لخضر الوادي

Echahid Hamma Lakhdar University Of El-Oued

كلية العلوم الطبيعة والحياة

Faculty Of Natural Sciences and Life

قسم العلوم الفلاحية

DEPARTMENT OF AGRICULTURAL SCIENCES

Master's Thesis

Submitted in Partial Fulfillment of the Requirements for the Degree of Master in Agronomic Sciences

Specialty: Plant Production

THEME

Use of Geographic Information Systems and Remote Sensing for Crop Analysis in a Saharan Environment: A Case Study of El Oued Province

Presented by: Dhikra REGUIEGUE

Roa NECIRA

Discussed on: 10/06/2026

Jury Members:

Chairman:	**Youcef HAKIMI**	**El-Oued University**
Supervisor:	**Samir MERDACI**	**El-Oued University**
Examiner:	**Ahmed ALLALI**	**El-Oued University**

Academic Year: 2025/2026

بسم الله الرحمن الرحيم

الإهداء

بسم الله الرحمان الرحيم، "**يرفع الله الذين آمنو منكم والذين أوتوا العلم درجات والله بما تعملون خبير**" صدق الله العظيم أولا وقبل كل شيء، أحمد الله حمدا كثيرا . . .فله الحمد أولا وآخرا، الحمد لله الذي هداني وسدد خطاي، الذي لم يتركني وحدي في أصعب اللحظات ، بهذا الحمد أبدأ، وبه أختم. اللهم بارك لي في علمي، وفيما سعيت من أجله، وفي كل لحظة تعبت فيها، وتقبله مني خالصا لوجهك الكريم، وصلي اللهم وسلم على سيدنا محمد صلى الله عليه وسلم.

إلى من أضاءوا ظلمة الطريق...

إلى من حملتني أحشاؤها تعباً فوق تعب، وأسهرت جفونها رجاء أن أراه يوماً في أعلى المراتب. . . إلى أمي: هذا الجهد ثمرة دعائك، وهذا النجاح هدية عرق جبينك.

إلى من كان ظهري الذي لا ينحني، وسندي الذي لا يتزعزع، وغصن الحلم الذي استظل به. . . إلى أبي: هذا العمل حصيلة تضحياتك، وهذا التفوق ثمرة تعبك.

إلى من كانوا عوناً بعد الله...

إلى إخوتي وأخواتي، شركاء دربي وداعمي خطاي. إلى كل من آمن بي حين لم أكن أؤمن بنفسي.

إلى من علمني حرفاً أو كلمة أو معنى. . . إلى أساتذتي الكرام، ومن مقدمهم المشرف الفاضل سمير مرداسي، الذي كان نعم الموجه والناصح الأمين.

إلى كل من ساهم في هذه الرحلة...

زملائي، أصدقائي، كل من مد لي يد العون أو كلمة تشجيع، أو دعوة صادقة في ظهر الغيب.

وخير ما أختم به...

رب زدني علماً، وارزقني عملاً صالحاً ينتفع به الناس. وآخر دعوانا أن الحمد لله رب العالمين.

ذكرى

الإهداء

﴿وَأَن لَّيْسَ لِلْإِنسَانِ إِلَّا مَا سَعَىٰ ۝ وَأَنَّ سَعْيَهُ سَوْفَ يُرَىٰ﴾

الفضل لله الذي جعل لي من الدرب نوراً، ومن السعي طريقاً للإنجاز، والحمد لله الذي ما تيقنت به خيراً وأملاً إلا وأغرقني سروراً وفرحاً، فلك الحمد يا الله حباً وشكراً وامتناناً.

أهدي هذا الإنجاز إلى من أحمل اسمه بكل فخر واعتزاز، إلى من غرس في قلبي حب العلم والطموح، إلى قدوتي ومثلي الأعلى، داعمي الأكبر وسندي الثابت الذي لا يميل . . . أبي الغالي.

إلى الدفء الدائم في حياتي، والطمأنينة وسط كل فوضى، إلى من بوجودها تصبح الأيام كلها أعياداً، وبدعواتها تزهر أيامي، إلى مأمن قلبي ورفيقة دربي الأولى . . . أمي الغالية.

إلى زوجي الكريم، شريك حياتي ورفيق دربي، الذي كان خير سندٍ وعونٍ لي طوال هذه المسيرة، والذي أحاطني بدعمه وتشجيعه وصبره، فكان حضوره مصدر قوة وأمان في كل مرحلة من مراحل هذا الإنجاز. شكراً لك على ثقتك الدائمة بي، وعلى كل كلمة تحفيز ومساندة قدمتها لي، وعلى محبتك واهتمامك اللذين كان لهما الأثر الكبير في مواصلة هذا المشوار وإتمامه. لك مني كل الشكر والتقدير والمحبة والامتنان.

إلى رياحين عمري ورفاق خطوتي الأولى، إخوتي وأخواتي الأعزاء، الذين يشاركونني الفرح ويغمرونني بحبهم ودعمهم، ويمنحونني من قوتهم ما يكفيني لأواصل الطريق، إلى من أفتخر بوجودهم في حياتي.

وإلى كل من يرافقني بنية طيبة، ومن يفرح لنجاحي كأنه نجاحه، ويتمنى لي كل الخير.

وأخيراً، كم من مرة شعرت أني لن أستطيع، ولكنها أنا اليوم، رغم كل شيء، قد أنهيت صفحات أثقلتها الكلمات والأفكار، وأكواب قهوة كانت رفيقتي في السهر.

أهدي هذا الإنجاز إلى نفسي، التي لم تقبل يوماً إلا بالتفوق والتميز، والتي آمنت بأحلامها وسعت لتحقيقها رغم كل الصعوبات والتحديات.

إلى كل هؤلاء أهدي ثمرة جهدي، راجيةً من الله أن يجعل فيها الخير والنفع والتوفيق.

رؤى

Acknowledgments

Praise be to Allah, the Almighty, who granted me success and enabled me to complete this work. Peace and blessings be upon our Prophet Muhammad (peace be upon him).

I extend my sincere gratitude, appreciation, and thankfulness to my supervisor, Mr. Samir Merdaci, for his excellent guidance, continuous follow-up, and valuable scientific advice, which greatly contributed to the completion of this thesis.

I also express my deep gratitude to the honorable members of the examination committee for kindly accepting to discuss and evaluate this work.

My thanks go to all the professors of the Department of Agricultural Sciences and to everyone who contributed, directly or indirectly, to the completion of this research, whether through advice, assistance, or encouragement.

Finally, I offer my heartfelt thanks and appreciation to my dear family for their support, patience, and encouragement throughout my academic journey.

And Allah is the Grantor of success.

Abstract

The Oued Souf region in southeastern Algeria has experienced significant agricultural expansion relying on center pivot irrigation, leading to severe groundwater depletion (a 30 m drop in the water table) and increased soil salinization. Although the Oued Righ region no longer administratively belongs to Oued Souf, it remains one of southern Algeria's most important agricultural areas due to its oasis system and date palm groves. This study aimed to employ remote sensing and GIS techniques to monitor barley as a strategic crop and to analyze the spatiotemporal dynamics of vegetation cover over the period 2016–2026, while testing the reliability of the Normalized Difference Vegetation Index (NDVI) for agricultural decision support.

The methodology integrated weekly field measurements of barley plant height from an experimental plot in Debila (February–May 2026) with NDVI values derived from Sentinel-2 imagery, together with a long-term time-series analysis of vegetation cover using seven spectral classes.

The results showed a strong relationship between NDVI and barley vertical growth ($R^2 = 0.905$). NDVI peaked at 0.67 in week nine, coinciding with maximum vegetative development, then declined as physiological maturity began. At the regional level, the 10-year analysis revealed that drought periods (2017–2025) caused a contraction of higher NDVI classes (>0.4) and an expansion of lower classes, while the exceptionally wet year 2026 showed marked recovery. The moderate vegetation class (0.2–0.4) peaked in 2021 with 6.15 million pixels, and the dense vegetation class (0.4–0.6) peaked in 2025 with 2.05 million pixels.

The study concludes that remote sensing and Geographic Information System GIS constitute an accurate and reliable alternative to costly field surveys. It recommends their adoption for agricultural and environmental monitoring, and the use of class-based frequency analysis rather than mean NDVI values alone.

Keywords: Remote Sensing, NDVI, Barley, Oued Souf, Vegetation Cover, Precision Agriculture.

Abstract in Arabic (الملخص)

شهدت منطقة وادي سوف، الواقعة في الجنوب الشرقي للجزائر، توسعًا زراعيًا كبيرًا قائمًا على الري المحوري (center pivot irrigation) ، ما ترتب عليه استنزاف حاد للمياه الجوفية تمثّل في هبوط منسوب المياه الجوفية بنحو 30 مترًا، وازدياد معدلات ملوحة التربة. ورغم أن منطقة وادي ريغ لم تعد تتبع إداريًا لوادي سوف، فإنها تظل واحدة من أبرز المناطق الزراعية في جنوب الجزائر، نظرًا لما تزخر به من نظام واحاتي وبساتين نخيل مثمرة. وقد هدفت هذه الدراسة إلى استخدام تقنيات الاستشعار عن بعد و. GIS في رصد محصول الشعير بوصفه محصولًا استراتيجيًا، وتحليل التغيّرات المكانية–الزمانية للغطاء النباتي في منطقة واد ريغ خلال الفترة الممتدة بين 2016 و2026، إلى جانب اختبار مدى جودة مؤشر NDVI وصلاحيته بوصفه أداة مساندة لصنع القرار الزراعي.

اعتمدت المنهجية على دمج القياسات الحقلية الأسبوعية لارتفاع نبات الشعير، التي أُجريت في قطعة تجريبية بمنطقة الدبيلة خلال الفترة الممتدة من فبراير إلى مايو 2026، مع قيم NDVI المستخلصة من صور القمر الصناعي Sentinel–2، بالإضافة إلى تحليل السلاسل الزمنية طويلة المدى للغطاء النباتي بالاستناد إلى سبع فئات طيفية.

أظهرت النتائج وجود علاقة قوية بين مؤشر NDVI والنمو الرأسي للشعير، إذ بلغ معامل التحديد (R^2) قيمة 0.905. وبلغت ذروة المؤشر قيمة 0.67 في الأسبوع التاسع، تزامنت مع أقصى مرحلة من التطور الخضري، أعقبها تناقص تدريجي في القيم مع دخول النبات في مرحلة النضج الفسيولوجي. وعلى المستوى الإقليمي، كشف تحليل المدة الزمنية البالغة 10 سنوات أن فترات الجفاف (الممتدة بين 2017 و2025) أدت إلى تقلّص رقعة الفئات الطيفية الأعلى قيمًا (>0.4) واتساع نطاق الفئات الأدنى، في المقابل، أظهر العام 2026، الذي اتسم بوفرة استثنائية في الهطولات المطرية، تعافيًا ملموسًا للغطاء النباتي. وبلغت فئة الغطاء النباتي المتوسط (0.2–0.4) ذروتها في عام 2021 بعدد 6.15 مليونpixels ، في حين سجّلت فئة الغطاء الكثيف (0.4–0.6) أقصى اتساع لها في عام 2025 بعدد 2.05 مليون.pixels

تستخلص الدراسة إلى أن تقنيات الاستشعار عن بعد ونظم المعلومات الجغرافية GIS تُشكّل بديلاً دقيقًا وموثوقًا عن المسوحات الميدانية الباهظة التكاليف، وتُوصي باعتمادها في مجالي الرصد الزراعي والبيئي، مع التأكيد على ضرورة توظيف التحليل التكراري القائم على التصنيف الطبقي (class–based frequency analysis) بدلاً من الاقتصار على قيم متوسط NDVI وحدها.

الكلمات المفتاحية :الاستشعار عن بعد، مؤشرNDVI ، الشعير، وادي سوف، الغطاء النباتي، الزراعة الدقيقة.

Abstract in French (Résumé)

La région de l'Oued Souf, dans le sud-est algérien, a connu une expansion agricole significative reposant sur l'irrigation par pivots centraux, entraînant un épuisement sévère des eaux souterraines (baisse de la nappe de 30 mètres) et une salinisation accrue des sols. Cette étude visait à utiliser la télédétection et les SIG pour suivre l'orge en tant que culture stratégique et analyser la dynamique spatio-temporelle du couvert végétal sur la période 2016–2026, tout en testant la fiabilité de l'indice de végétation par différence normalisée (NDVI) pour l'aide à la décision agricole.

La méthodologie a intégré des mesures hebdomadaires de terrain de la hauteur des plants d'orge dans une parcelle expérimentale à Debila (février–mai 2026) avec les valeurs NDVI extraites d'images Sentinel-2, ainsi qu'une analyse chronologique à long terme du couvert végétal utilisant sept classes spectrales.

Les résultats ont montré une forte relation entre le NDVI et la croissance verticale de l'orge (R^2 = 0,905, r = 0,88). Le NDVI a atteint un pic de 0,67 à la neuvième semaine, coïncidant avec le développement végétatif maximal, puis a diminué avec le début de la maturité physiologique. À l'échelle régionale, l'analyse sur 10 ans a révélé que les périodes de sécheresse (2017–2025) ont provoqué une contraction des classes NDVI supérieures (>0,4) et une expansion des classes inférieures, tandis que l'année exceptionnellement humide 2026 a montré une nette reprise. La classe de végétation modérée (0,2–0,4) a culminé en 2021 avec 6,15 millions de pixels, et la classe de végétation dense (0,4–0,6) a culminé en 2025 avec 2,05 millions de pixels.

L'étude conclut que la télédétection et les Système d'Information Géographique SIG constituent une alternative précise et fiable aux coûteuses enquêtes de terrain. Elle recommande leur adoption pour la surveillance agricole et environnementale, ainsi que l'utilisation d'une analyse de fréquence basée sur les classes plutôt que des seules valeurs moyennes du NDVI.

Mots-clés : Télédétection, NDVI, Orge, Oued Souf, Couvert végétal, Agriculture de précision.

Table of Content

الإهداء I

الإهداء II

Acknowledgments III

Abstract IV

Abstract in Arabic (الملخص) V

Abstract in French (Résumé) VI

Table of Content VII

Liste of Abbreviation X

Liste of figure XII

Liste of Tables XIII

FIRST PART Theoretical section

CHAPTER I: Remote Sensing

1.1Concept of remote sensing in agriculture: 5

1.2 Physical fundamentals: (electromagnetic spectrum, interaction with vegetation). 5

1.2.1. Electromagnetic Spectrum 6

1.2.2. Interaction with vegetation: 8

1.2.3. Evolution of satellite systems: 9

.... 10

2.1. Multi-Spectral Imaging 11

2.2 Hyperspectral Imaging 11

3.1 Fundamental Concepts of Crop Analysis 11

3.1.1. Types of Crops and Growth Requirements 11

3.1.2. Crop Life Cycle and Environmental Relationships 12

3.2. Spectral Indices for Crop Assessment 12

3.2.1. Vegetation index 12

3.2.2. Normalized Difference Vegetation Index (NDVI) 13

3.2.3. Other Key Spectral Indices (SAVI, NDWI) 14

4. Applications of GIS and Remote Sensing in Precision Agriculture 15

4.1. Crop Area Estimation and Classification 15

4.2. Crop Monitoring and Stress Detection 15

4.2.1Water Stress Detection: 15

4.2.2Pest and Disease Detection: 15

4.3. Yield Estimation 16

4.4. Water Resource Management 17

CHAPTER II:The Conceptual Framework of Geographic Information Systems (GIS)

1.Geographic Information Systems (GIS) 18
1.1. Definition and Historical Development of GIS 18
1.1.1. Definition of GIS: 18
1.1.2. History of Geographic Information System: 18
1.2. Components of a Geographic Information System 18
1.3. Types of Spatial Data: Raster and Vector 19
1.3.1 Geographic Data: 19
1.3.2Vector Data: 19
1.3.3 Raster Data: 20
1.4 Core Spatial Analysis Functions 20
1.5 Q GIS 21

CHAPTER III: STUDY OF THE REGION

1.Geographical Location 24
2. Study area 24
3.1. Topographic Nature of the Study Area 24
3.2. Terrain Slope 25
4. Climate 26
4.1. Temperature 26
4.2 Relative Humidity 27
4.3. Wind 27
4.4 Rainfall 27
5.1 Bagnouls and Gaussen ombrothermic diagram: 28
5.2 Emberger climagram 28
6. Natural characteristics 30
6.1. Natural zone 30
6.2. Geographical zone 31
7. Water resource potential of the wilaya 31
7.1. The groundwater aquifers found in this region are as follows 31
7.2. Surface water resources 32
8 . Social, cultural and economic activity 32
9. General type of agriculture 32

SECOND PART:Applied section

CHAPTER I: Study of The Barley Crop using NDVI

1.1 Study Site ...35
1.2 Crop Material ...35
1.3 Measurement Equipment ...36
2. Method: ...36
2.1 Field Sampling ...36
2.2 Plant Height Measurement ...36
1.1 Satellite Data Source ...39
1.2 Processing Software ...39
1.3 Spatial Area of Interest (Satellite) ...40
2. Method ...40
2.1 Downloading Satellite Images from Copernicus ...40
2.2 NDVI Calculation Using QGIS ...41
2.3 Extracting NDVI Values for the Barley Field (10×10 m pixel) ...42
2.4 Plotting the NDVI Curve Using Excel ...43
3. Results: ...44
4. Discussion: ...46

CHAPTER II Case Study (OUED RIGH)

1.2 Satellite Data (Sentinel-2 Dataset) ...50
3. Calculation and Analysis of the NDVI Spectral Index: ...51
4.1 NDVI Class Distribution (2016–2026) ...51
4.1.1 High NDVI Classes (NDVI > 0.4) – Healthy, Dense Vegetation ...52
4.1.2 Moderate NDVI Class (0.2–0.4) – Moderate Vegetation ...52
4.1.3 Low NDVI Class (0–0.2) – Bare Soil / Weak Vegetation ...53
4.1.4 Negative NDVI Classes (NDVI < 0) ...53
4.2 Temporal Trajectory of NDVI Classes ...53
5.1 Relationship Between Climatic Variability and NDVI Distribution ...55
5.2 Impact of the Prolonged Drought Period (2017–2025) ...55
5.3 Vegetation Recovery Following the 2026 Extreme Rainfall Event ...55
5.4 Non-Instantaneous Nature of the NDVI–Precipitation Relationship ...55
5.5 Overall Consistency and Utility of NDVI as a Monitoring Tool ...56
Conclusion ...57
References ...61

Liste of Abbreviation

- **GIS** – Geographic Information System
- **NDVI** – Normalized Difference Vegetation Index
- **MODIS** – Moderate Resolution Imaging Spectroradiometer
- **SAR** – Synthetic Aperture Radar

EMR – Electromagnetic Radiation

- **Hz** – Hertz
- **UK** – United Kingdom
- **BRDF** – Bidirectional Reflectance Distribution Function
- **ERTS** – Earth Resources Technology Satellite (original name for Landsat 1)
- **HSI** – Hyperspectral Imaging
- **IR** – Infrared
- **IRS** – Indian Remote Sensing satellite
- **LAI** – Leaf Area Index
- **MIR** – Mid-Infrared
- **MSI** – Multispectral Imaging
- **NASA** – National Aeronautics and Space Administration (USA)
- **NIR** – Near-Infrared
- **RED** – Red band (reflectance in red wavelength)
- **SPOT** – Satellite Pour l'Observation de la Terre (France)
- **TIROS** – Television Infrared Observation Satellite
- **USGS** – United States Geological Survey
- **VI** – Vegetation Index
- **VIS** – Visible spectrum (implied, but not explicitly defined in this excerpt)
- **CGIS** – Canada Geographic Information System
- **CWSI** – Crop Water Stress Index
- **DSSAT** – Decision Support System for Agrotechnology Transfer
- **ET** – Evapotranspiration
- **EVI** – Enhanced Vegetation Index
- **GNDVI** – Green Normalized Difference Vegetation Index
- **LAI** – Leaf Area Index
- **LST-VI** – Land Surface Temperature – Vegetation Index
- **METRIC** – Mapping Evapotranspiration at High Resolution with Internalized Calibration

- **NDRE** – Normalized Difference Red Edge
- **NDWI** – Normalized Difference Water Index
- **OPTRA**M – OPtical TRApezoid Model (referenced as OPTRAM model)
- **OSAVI** – Optimized Soil-Adjusted Vegetation Index
- **PLSR** – Partial Least Squares Regression
- **PRI** – Photochemical Reflectance Index
- **RMSE** – Root Mean Square Error
- **SAVI** – Soil-Adjusted Vegetation Index
- **SEBAL** – Surface Energy Balance Algorithm for Land
- **STICS** – Simulateur mulTIdisciplinaire pour les Cultures Standard (a crop growth model)
- **SVM** – Support Vector Machine
- **TDR** – Time Domain Reflectometry
- **UAV** – Unmanned Aerial Vehicle
- **WOFOST –** World Food Studies (crop growth simulation model)
- **API** – Application Programming Interface
- **GDAL** – Geospatial Data Abstraction Library
- **GRASS** – Geographic Resources Analysis Support System
- **PyQGIS** – Python for QGIS
- **QGIS** – Quantum Geographic Information System (open-source GIS software)
- **SAGA** – System for Automated Geoscientific Analyses
- **WFS** – Web Feature Service
- **WMS** – Web Map Service
- **DSA** – Direction des Services Agricoles (Directorate of Agricultural Services)
- **AOI** – Area of Interest
- **ESA** – European Space Agency
- **GPS** – Global Positioning System
- **S2L2A** – Sentinel-2 Level 2A (collection)
- **S2MSI2A** – Sentinel-2 MultiSpectral Instrument Level 2A (product type)
- **SWIR** – Shortwave Infrared

Liste of figure

Figure 01:EM Interactions with Matter transmission; (b (Omia et al., 2023)................................7

Figure 02: The Electromagnetic Spectrum and Its Agricultural Applications (Omia et al., 2023)...8

Figure 03: Spectral Response Curves of Water, Soil, and Vegetation. (Kumawat et al., 2023a) 9

Figure 04: Absorbance spectra of plant photosynthetic pigments at different wavelengths ranges (Kumawat et al., 2023a)..9

Figure 05: Types of Geographic Data in a GIS. 19

Figure 06: Representation of Thematic Layers 20

Figure 07: Geographic location of the El Oued region (Produced by QGIS) 24

Figure 08: Topographic map of the El Oued valley 26

Figure 09: Bagnouls and Gaussen ombrothermic diagram..28

Figure 10: Location of the El Oued region on the climagram 30

Figure 11: Barley Field Location 35

Figure 12: Barley Pivot...35

Figure 13: Barly 08/03/2026 37

Figure 14: Barley 18/03/2026 37

Figure 15: Barley 06/04/2026 38

Figure 16: Barley 12/05/2026 38

Figure 17: 39

Figure 18: Copernicus 39

Figure 19: Downloading Satellite Images from Copernicus 41

Figure 20: NDVI Calculation Using QGIS..42

Figure 21: NDVI Values..42

Figure 22: Excel...43

Figure 23:Temporal Curves of Weekly NDVI Values and Barley Plant Height (cm) 44

Figure 24:Scatter Plot with Second-Degree Polynomial Trendline: NDVI vs. Plant Height....45

Figure 25: NDVI Map of Barley Vegetation Cover 46

Figure 26: location map of study area Oued Righ..49

Figure 27: NDVI Map of the Oued Righ Region(2026–2016) 51

Figur 28:Temporal Curves of NDVI Values and Pixel Count Distribution(2026–2016) 54

Figure 29: Bar Chart of Temporal Changes in NDVI Values and Pixel Counts(2026–2016) ...54

Liste of Tables

Table 1:Broad categorization of the electromagnetic spectrum.(Omia et al., 2023) 6

Table 2. Satellites with High Spatial and Temporal Resolution for Agriculture(Sishodia et al., 2020a) 10

Table 3. Spectral Vegetation Indices in Precision Agriculture (Kumawat et al., 2023a) 14

Table 4: Average altitude of the different municipalities of the El Oued (Cité par, TOUATI, ABBIDI ,2018). 25

Table 5: Average monthly temperatures of the El Oued region during the period 2013–2023 Source (ONM)... 27

Table 6: Average monthly humidity of the El Oued region during the period 2013–2023 Source (ONM)... 27

Table 7 : Average monthly wind speed of the El Oued region during the period 2013–2023 . 27

Table 8: Average monthly precipitation in the El Oued region during the 2013–2023 period 27

Table 9 : Pixel Coordinates 36

Table 10: Evolution of average plant height: 36

Table 11: NDVI and Plant Height (cm) by Week.. 44

Table 12: Pixel Count Distribution Across NDVI Classes (2016–2026) 52

INTRODUCTION

Oued Souf region in southeastern Algeria represents a striking example of agricultural transformation in arid environments. This area has shifted from traditional subsistence farming to intensive commercial agriculture, largely driven by the adoption of center-pivot irrigation systems. Between 2005 and 2016. the irrigated agricultural area more than doubled, expanding from 12,200 ha to 31,700 ha.1(Abdaoui et al., n.d.). However, this expansion has given rise to serious environmental challenges, most notably the overexploitation of groundwater resources. Between 2016 and 2021, groundwater levels dropped by as much as 30 meters. In addition , soil salinization has intensified due to the use of highly saline water for irrigation(Tarek et al., 2025; Zaiz & Boutoutaou, 2022).

In light of these challenges, there is an urgent need to adopt modern agricultural practices and real-time, high-resolution crop monitoring. Remote sensing techniques and Geographic Information Systems (GIS) are among the most important tools available to achieve this. Numerous studies have demonstrated the effectiveness of the Normalized Difference Vegetation Index (NDVI), derived from satellite imagery (MODIS, Landsat, Sentinel-2), in predicting cereal crop yields in semi-arid regions of North Africa. A strong correlation has been observed between NDVI values and agricultural yields, enabling reliable yield predictions two to three months before harvest.(Boulaaras & Bouregaa, 2024)

These techniques have also been successfully applied in neighboring Algerian regions, such as Biskra and Khenchela, for crop classification and vegetation health monitoring. Using machine learning algorithms applied to SAR data and optical imagery, classification accuracies exceeding 85% have been achieved.(Mayouf et al., 2025)

In the Béchar region, a precision irrigation system based on multispectral indices derived from Sentinel-2 and Landsat 8 satellites has been developed. This system has demonstrated the potential to reduce water consumption by up to 30% without compromising crop productivity.(Benyamina & Hanane, 2025)

Despite these promising applications, the adoption of precision agriculture in Algeria still faces several obstacles. According to a survey involving 322 Algerian agricultural engineers, the main barriers include the high cost of the technologies involved, the limited availability of qualified labor, and the lack of market access to many of these technologies within Algeria(Soum et al., 2025).

In this context, this study aims to utilize Geographic Information Systems (GIS) and remote sensing to monitor and analyze barley crops in the Souf Valley region and to carry out the study of Oued Righ. These tools are intended as a real-time monitoring framework to improve resource management and optimize the use of natural assets, thereby supporting the national vision for achieving food security and self-sufficiency in strategic crops.

Problematic:

Given the importance of monitoring barley growth as a strategic crop in the Oued Righ region (Ouadi Souf), and the lack of periodic spatial studies assessing vegetation cover over a decade, the following problem arises:

How can remote sensing and GIS techniques, specifically the NDVI index, be used to monitor the growth of a barley crop in an experimental field (in the Debila area) and to track changes in vegetation cover across the entire Oued Righ region during the period from 2016 to 2026, and can the results obtained be relied upon for agricultural decision making and for predicting future crop status?

From this main problem, the following sub questions emerge:

1. What is the growth curve of barley under center pivot irrigation as revealed by field measurements and spectral indices?
2. How has vegetation cover in the Oued Righ region evolved in terms of area and green density during the last ten years (2016–2026)?
3. Is there a strong correlation between field measurements (barley plant height) and NDVI values extracted from satellite images, and what is the accuracy of this relationship?
4. Which areas in Oued Righ are most prone to vegetation cover degradation?
5. Do remote sensing techniques prove their effectiveness in providing accurate results that can serve as a reliable alternative (or complement) to intensive field surveys for prediction and agricultural decision making?

Study Objectives

This work aims to achieve the following:

General objective:

To demonstrate the ability of remote sensing techniques (NDVI index) to provide accurate and reliable results that can be used for predicting vegetation cover status and supporting agricultural decision making, through a case study of barley in the Oued Righ region.

Specific objectives:

1. Establish the seasonal growth curve of barley using weekly field measurements (height) from an experimental field in Debila, and compare them with NDVI values extracted from satellite images for the same period (February – May 2026).

2. Analyze the temporal changes in vegetation cover across the Oued Righ region over a long term period (10 years: 2016–2026) using a time series of satellite images (e.g., Sentinel 2 or Landsat) and the NDVI index.

3. Identify stable and degraded vegetation areas within the study region and classify them according to change intensity (increase, decrease, stability).

4. Relate changes in vegetation cover to environmental factors (salinity, soil type, irrigation systems) based on available pedological maps.

5. Assess the accuracy and reliability of the NDVI index by comparing its values with actual field measurements (plant height), calculating the coefficient of determination (R^2) or other error indicators, in order to prove that remote sensing can be used as a tool for prediction and agricultural advisory.

6. Provide practical recommendations to farmers in the Oued Righ region (Ouadi Souf) on how to use the NDVI index for monitoring their crops and for identifying areas that require early agricultural intervention (e.g., fertilization or irrigation adjustment).

FIRST PART

Theoretical section

CHAPTER I

Remote Sensing

1.1Concept of remote sensing in agriculture:

“The science of gaining information about an object through the analysis of data obtained by a device that is not in contact with the object is known as remote sensing” . In other words, remote sensing is the science of gathering and evaluating information about the environment using sensors that are not in physical touch with the environment (National Remote Sensing Centre - UK) . The phrase "remote sensing" refers to a group of techniques for detecting the chemical or physical qualities of physical objects at any distance by recording, measuring, and interpreting images and digital representations of energy patterns generated by non-contact sensor systems.

The interaction of electromagnetic radiation released by the sun with soil and plant material is the basis for remote sensing in agriculture. Sensors are the instruments that are used to measure electromagnetic radiation. Sensors, film cameras, digital cameras, and video recorders may be used to collect data from various platforms such as satellites, aircrafts, drones, tractors, and in the form of manual handheld radiometers . Instead of measuring transmitted and absorbed electromagnetic radiation, optical remote sensing sensors monitor the incoming electromagnetic radiation from the sun and the present of electromagnetic radiation reflected by the earth's surface materials. The physical and chemical composition of the material existing on the earth's surface to which solar radiation is incident determines the degree of absorption, reflection, and transmission . Refection spectra, or characteristic refection curves, are the outcome of this. With the help of these spectra, which plot the refection against the wavelength of electromagnetic radiation, we may detect the materials present on the surface and partially characterize their condition..(Kumawat et al., 2023a)

1.2 Physical fundamentals: (electromagnetic spectrum, interaction with vegetation).

At the physical level, the principle is uncomplicated: matter does not engage with light uniformly across the spectrum. Healthy green flora predominantly absorbs significant quantities of red and blue wavelengths due to the presence of chlorophyll, while it predominantly reflects green wavelengths—this phenomenon accounts for its green appearance—and exhibits an even greater reflection of near-infrared radiation attributable to the structural composition of the leaf tissue. These spectral variances are instrumental in rendering indices such as NDVI and others practicable, and they further elucidate the reasons behind signal variations in correlation with growth, water deficiency, disease manifestations, and senescence.(Avery, 2018)

1.2.1. Electromagnetic Spectrum

Remote sensing technology depends on the measurement and interpretation of **EMR** arrays. This radiation carries specific electrical and magnetic properties. We refer to the wavelength range that corresponds to the electromagnetic radiation as the electromagnetic spectrum. We can use the manner of the interaction between the electromagnetic spectrum with any material for the qualitative and quantitative analyses of various materials. Researchers often use the electromagnetic spectrum to analyze the various chemical and physical properties of food and agriculture materials . The electromagnetic spectrum ranges from shorter wavelengths (including gamma and X-rays) to longer wavelengths (including microwaves and broadcast radio waves), as detailed in **Table 1**. The three basic factors that define the electromagnetic spectrum are the frequency (f), wavelength (λ), and photon energy (E). The frequency refers to the number of cycles per unit time, which are measured in hertz (Hz) (number of cycles per second). The wavelength refers to the distance between two successive cycles, which is measured in meters (m), and which is inversely proportional to the frequency. The following equations describe the relationships between the frequency, wavelength, and energy:

$$f = \frac{c}{\lambda'} \cdot \cdots\cdots\cdots\cdots (1)$$

$$f = \frac{E}{h'} \cdots\cdots\cdots\cdots\cdots (2)$$

$$E = \frac{hc}{\lambda'} \cdots\cdots\cdots\cdots\cdots\cdots (3)$$

where h is the Planck's constant (6.6206957 × 10-34), and c is the speed of light in a vacuum (299,792,458 m/s).(Omia et al., 2023)

Table 1:Broad categorization of the electromagnetic spectrum.(Omia et al., 2023)

Broad Category	Wavelength (m) (Low to High)	Frequency (Hz) (High to Low)
Gamma radiation	$< 10^{-11}$	$> 3 \times 10^{19}$
X-ray radiation	$10^{-9} - 10^{-11}$	$3 \times 10^{17} - 3 \times 10^{19}$
Ultraviolet radiation	$4 \times 10^{-7} - 10^{-9}$	$7.5 \times 10^{14} - 3 \times 10^{17}$
Visible radiation	$7 \times 10^{-7} - 4 \times 10^{-7}$	$4.3 \times 10^{14} - 7.5 \times 10^{14}$
Infrared radiation	$1 \times 10^{-5} - 7 \times 10^{-7}$	$3 \times 10^{12} - 4.3 \times 10^{14}$
Microwave radiation	$0.01 - 10^{-5}$	$3 \times 10^{9} - 3 \times 10^{12}$
Radio waves	> 0.01	$< 3 \times 10^{9}$

Depending on the type of interaction with the object **(Figure 1),** we can use the electromagnetic spectrum in different types of spectroscopic techniques to study material properties. The most applied interaction types for agricultural applications include reflectance, where the radiation is bounced back in either regular or irregular directions; ab-sorption, where the electromagnetic radiation is absorbed by the object (e.g., in photosynthesis); transmission, where the object allows the passage of electromagnetic radiation; emission, where the object emits the electromagnetic radiation that is the result of an energy state transition (e.g., fluorescence).(Omia et al., 2023)

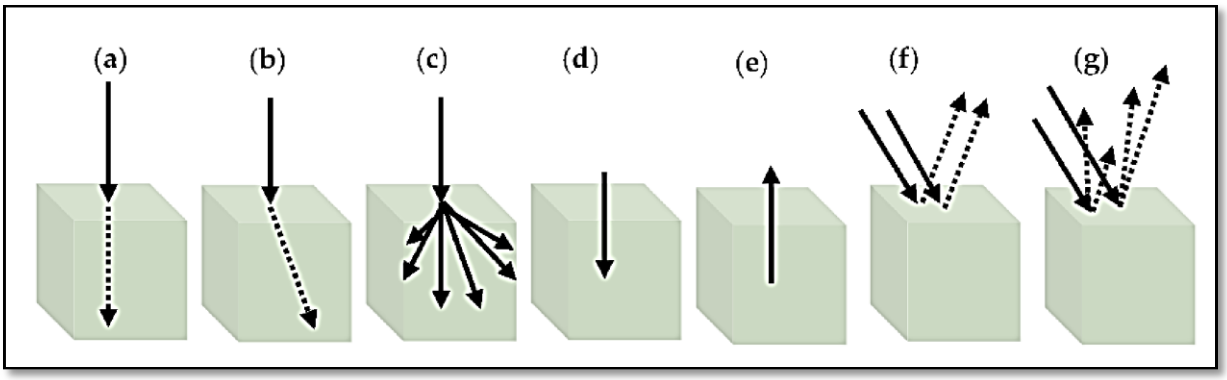

Figure 01:EM Interactions with Matter transmission; (b (Omia et al., 2023)

The information associated with each region in the electromagnetic spectrum can be helpful for a particular purpose for understanding field crops. The visible spectrum (0.4–0.7 µm) is used for vision-based sensing (i.e., measures to quantify all valuable data observable by the naked eye), such as chlorophyll studies, green indices, and morphological analyses of leaves and fruits . Similarly, the infrared region (0.3–100 µm) is used to extract data that are hidden from the naked eye, such as the plant water content and stress-related indices. However, the infrared (IR) spectrum that is used in remote sensing comprises two subcategories, based on the radiation properties: (1) the reflected IR spectrum (0.7–3.0 µm), which is used for remote sensing purposes in a similar manner to the visible spectrum; (2) the emitted or thermal IR spectrum (3.0–100 µm), which is radiation that is emitted from the Earth’s surface in the form of heat energy.

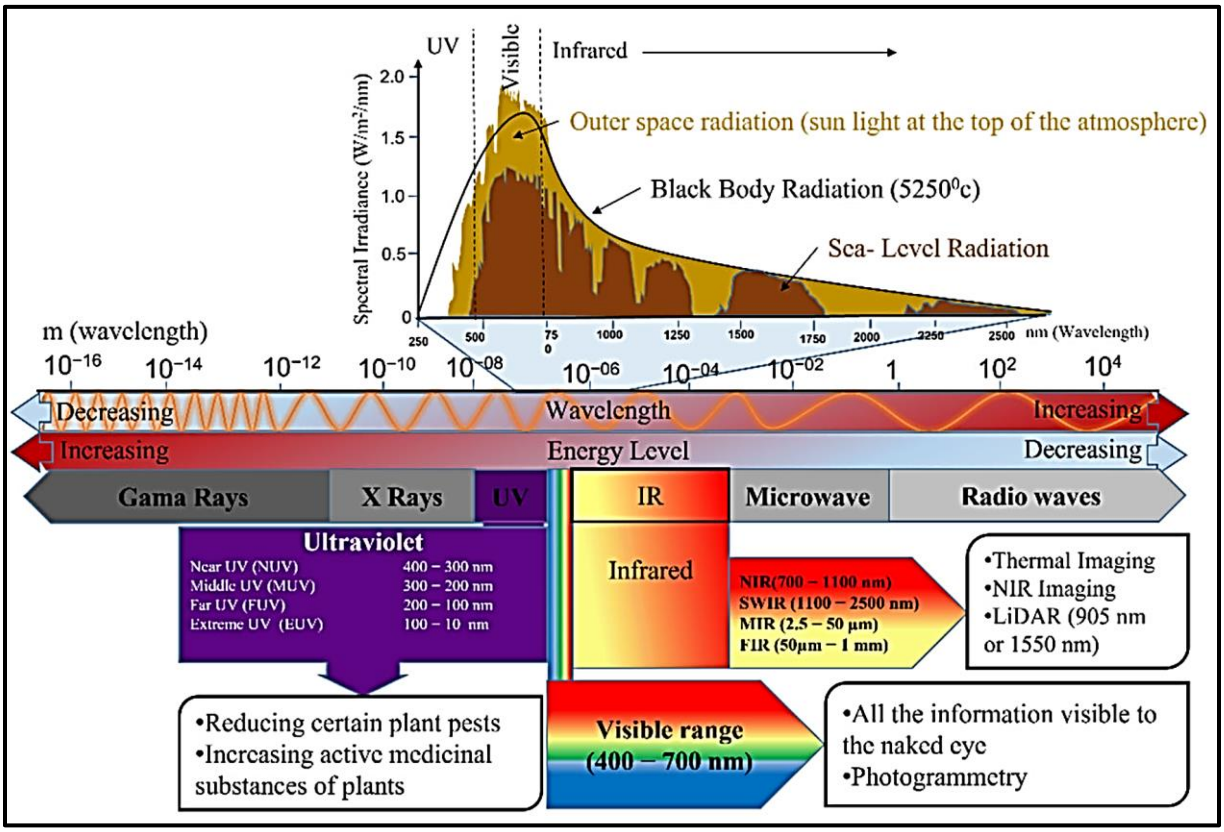

Figure 02: The Electromagnetic Spectrum and Its Agricultural Applications (Omia et al., 2023)

1.2.2. Interaction with vegetation:

Spectral signature of vital vegetation differs from dry vegetation, water and soil (**Fig. 3**) showed that the water bodies were absorb more effectively all wavelengths longer than the visible range while the green vegetation surface has produced a very specific spectral signature. Spectral signature of vegetation is based on the amount of radiation reflected from plants is inversely related to radiation absorbed by plant pigments (chlorophyll a, chlorophyll b, carotenoids) and varies with the wavelength of incident radiation. Plant pigments such as chlorophyll absorb radiation strongly at the visible spectrum from 400 to 700 nm . (**Fig. 4**). In contrast, plant reflectance is high in the near infrared (NIR 700 to MIR 1300 nm) region as a result of leaf density and canopy structure effects. The behavior of the NIR reflectance is also a function of leaf area index (LAI), cell turgor, leaf thickness, leaf internal air and water content.(Kumawat et al., 2023a). and it shows the reflectance % is low in the visible range (400- 700nm) due to (Kumawat et al., 2023a)

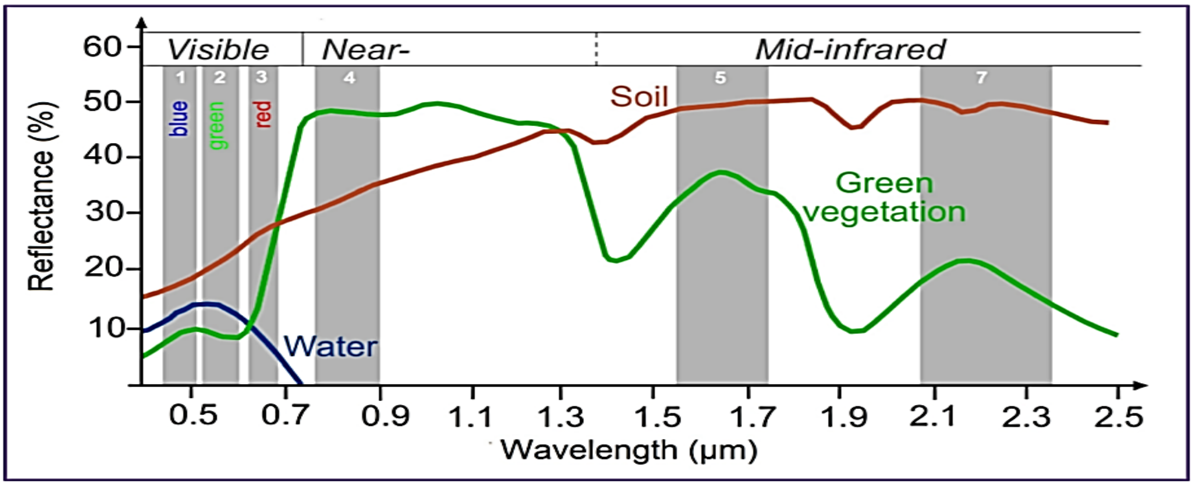

Figure 03: Spectral Response Curves of Water, Soil, and Vegetation. (Kumawat et al., 2023a)

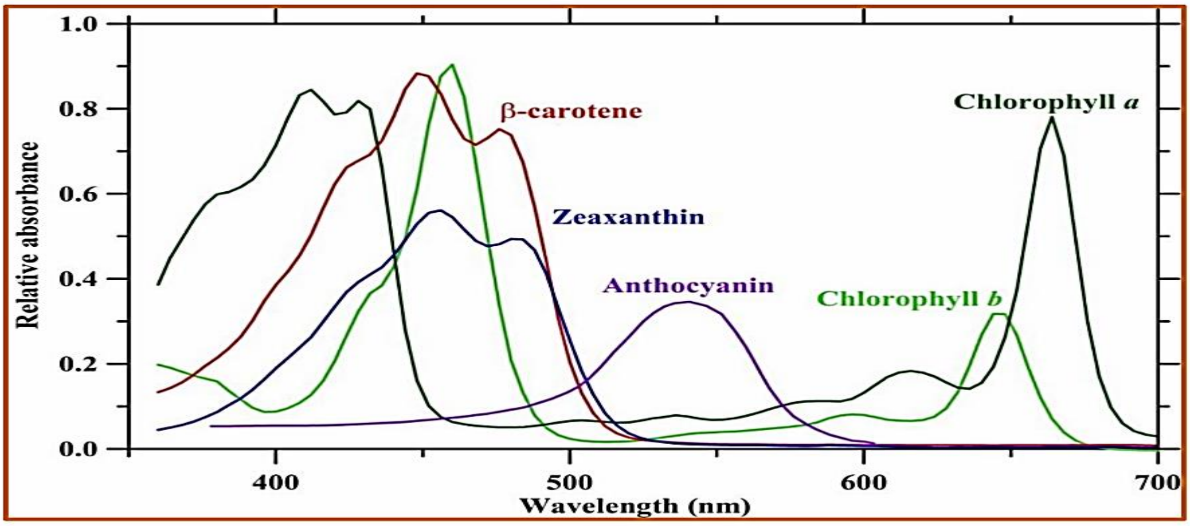

Figure 04: Absorbance spectra of plant photosynthetic pigments at different wavelengths ranges (Kumawat et al., 2023a)

1.2.3. Evolution of satellite systems:

Researchers have long emphasized the importance of mapping soil and land use databases for sustainable natural resource management at local, regional, and national scales. Understanding soil properties is crucial for designing irrigation, drainage, and nutrient strategies in precision agriculture, while land use mapping helps evaluate management and policy impacts. Although aerial photography was used for soil and crop mapping as early as the 1930s–1940s, traditional methods were labor-intensive, costly, and time-consuming. The advent of satellite remote sensing later enabled more efficient and effective mapping of land use and land cover across larger scales.

The launch of Vanguard 2 (1959) and TIROS 1 (1960) marked the beginning of satellite remote sensing for meteorological purposes. However, agricultural satellite remote sensing began with Landsat 1 (ERTS) launched by NASA on July 23, 1972. The Landsat program, jointly managed by NASA and the USGS, was followed by satellites Landsat 2–8, providing high-quality images for global natural resource management. Landsat images have been widely used for land use and crop classification, monitoring, and irrigation water requirement estimation. In 1984, Landsat 5 Thematic Mapper offered higher resolution (30 m) in more visible and NIR bands. Landsat 9 is planned for launch by mid-2021. Additionally, France launched SPOT 1 (1986) and India launched IRS-1A (1988).(Sishodia et al., 2020a)

Table 2. Satellites with High Spatial and Temporal Resolution for Agriculture(Sishodia et al., 2020a)

Satellite (Years Active)	Sensor (Spatial Resolution)	Temporal Resolution	Application in Precision Agriculture
Landsat 1 (1972–1978)	MS (80 m)	18 days	Crop growth [76]
AVHRR (1979–present)	MS (1.1 km)	1 day	Nutrient management [77]
Landsat 5 TM (1984–2013) Landsat 7 (1999–present) Landsat 8 (2013–present)	MS and Thermal (60 m–Landsat 7, 100 m–Landsat 8, 120 m–Landsat 5)	16 days	Biomass [78]; crop yield [79]; crop growth [80]
SPOT 1 (1986–1990) SPOT-2 (1990–2009)	MS (20 m)	2–6 days	Water management [81]
IRS 1A (1988–1996)	MS (72 m)	22 days	Water management, nutrient management [82]
LiDAR (1995)	VIS (10 cm)	N/A	Topography, nutrient management [83]
RadarSAT (1995–2013)	C-band SAR (30 m)	1–6 days	Crop growth [84]
IKONOS (1999–2015)	MS (3.2 m)	3 days	Crop yield [85]; soil properties [86]; nutrient management [77]; ET estimation [87]
EO-1 Hyperion (2000–2017)	HS (30 m)	16 days	Disease [88,89]
Terra/Aqua MODIS (Terra-1999–present, Aqua-2002–present)	MS (SpectroRadiometer; 250–1000 m)	1–2 days	Crop yield [90]; crop growth [91]
Terra-ASTER (2000–present)	MS and Thermal (15 m–V, NIR, 30 m–SWIR, 90 m–TIR)	16 days	Water management [92]
QuickBird (2001–2014)	MS (2.44 m)	1–3.5 days	Disease [93]
AQUA AMSR-E (2002–2016)	MS (Microwave Radiometer; 5.4 km–56 km)	1–2 days	Water management [94]
Spot-5 (2002–2015)	MS (V, NIR–10 m, SWIR–20 m)	2–3 days	Crop yield [95]
ResourceSat-1 (2003–2013)	MS (5.6m–V, 23.5 m–SWIR)	5 days	Nutrient management [96]
KOMPSAT-2 (2006–present)	MS (4 m)	5.5 days	Crop yield [97]
Radarsat-2	C-band SAR (1–100 m)	3 days	LAI and biomass [98]
RapidEye (2008–present)	MS (6.5 m)	1–5.5 days	Water management [99]; crop yield [100]; crop growth and chlorophyll [101]
GeoEye-1 (2008–present)	MS (1.65 m)	2.1–8.3 days	Nutrient management [102]
WorldView-2 (2009–present)	MS (1.4 m)	1.1 days	Crop growth [103]
Pleiades-1A (2011–present) Pleiades-1B (2012–present)	MS (2 m)	1 day	Crop growth [104,105]
VIIRS Suomi-NPP (2011–present) VIIRS-JPSS-1 (2017–present)	MS (IR Radiometer, 375 m and 750 m)	16 day (repeat)	Crop management (NDVI [106])
KOMPSAT-3 (2012–present)	MS (2.8 m)	1.4 days	Crop growth [107]
Spot-6 (2012–present), Spot-7 (2014–present)	MS (6 m)	1-day	Disease [108]
SkySat-1 (2013–present) SkySat-2 (2014–present)	MS (1 m)	sub-daily	Crop growth [109]
Worldview-3 (2014–present)	SS (1.24 m)	<1 day	Crop growth [110]; weed management [102]
Sentinel-1 (2014–present)	C-band SAR (5–40 m)	1–3 days	Crop growth
Sentinel-2 (2015–present)	MS (10 m–V and NIR, 20 m–Red edge and SWIR, 60 m–2 NIR)	2–5 days	Yield [111]; N management [112]
KOMPSAT-3A (2015–present)	MS (V NIR–2.2 m, SWIR–5.5 m)	1.4 days	Disease [113]
SMAP (2015–present)	L-band SAR (1–3 km) and radiometer (40 km)	2–3 days	Crop yield [114]; water management [115]
TripleSat (2015–present)	MS (3.2 m)	1 day	Crop growth [116]
ECOSTRESS-PHyTIR (2018–present)	Thermal (38 × 69 m)	1–5 days	ET [117]

2.1. Multi-Spectral Imaging

Multispectral imaging (MSI) captures several image layers of a scene, each corresponding to a specific spectral band. Most MSI sensors measure 3–10 bands per pixel. Examples include Landsat 8 (9 bands, 30 m resolution) and other satellites like Sentinel, Quickbird, and Spot, covering wavelengths from 443–2190 nm (ultra-blue to SWIR). MSI is widely used in field crop monitoring for applications such as biomass phenotyping, assessing reproductive organ effects on BRDF and NDVI, estimating photosynthetic pigments, and evaluating nitrogen variability. Additional agricultural uses include seed phenotyping for quality grading, soil nutrient estimation, and monitoring chlorophyll content. MSI has also enabled integration with machine learning and big data. However, limitations include the low number of discrete spectral bands and color restoration issues due to visible/NIR band overlap. Despite these drawbacks, MSI remains more commonly used than hyperspectral imaging (HSI) in remote sensing for crop monitoring, as HSI processing techniques are still under development.(Omia et al., 2023)

2.2 Hyperspectral Imaging

Hyperspectral imaging (HSI) captures dozens or hundreds of narrow, contiguous spectral bands for each pixel, unlike multispectral imaging (MSI) which collects only a few discrete bands. HSI has been shown to outperform MSI in various agricultural applications, such as digital soil mapping and detection of citrus gummosis, due to its ability to retrieve detailed spectral signatures. Because HSI acquires a full spectrum per point, no prior knowledge of the scene is required, and postprocessing can extract all available information. HSI also benefits from spectral-structural relationships in neighboring areas, improving classification accuracy. A known issue with HSI is the "smile" or "frown" effect, a spectral distortion primarily associated with push-broom sensors. Beyond agriculture, HSI is also applied in medical diagnosis and facial recognition.(Omia et al., 2023)

3.1 Fundamental Concepts of Crop Analysis

3.1.1. Types of Crops and Growth Requirements

Crop productivity depends on a complex set of interacting factors, including crop type, soil type, climatic events, soil fertility, water supply, nutrient availability, solar radiation duration throughout the growing season, and seeding rate.(Kumawat et al., 2023a)

The nature of agricultural traits can be categorical (e.g., crop type), physical (e.g., canopy temperature), chemical (e.g., leaf nitrogen content), biological (e.g., phenology), structural (e.g., leaf inclination angle), or geometric (e.g., plant density).(Weiss et al., 2020)

In the Abu Ghraib district of Iraq, climatic data indicated that mean annual temperatures are conducive to the growth of various crop types, including both winter and summer crops, and that available solar radiation supports differentiated crop growth patterns(Mahmood & Al-Rawe, 2023)

3.1.2. Crop Life Cycle and Environmental Relationships

The crop life cycle is closely linked to surrounding environmental factors. The fundamental processes governing crop performance include: light use efficiency and assimilate partitioning, energy balance, water balance (comprising soil evaporation and plant transpiration), carbon balance (photosynthesis and respiration), and nitrogen balance(Weiss et al., 2020)

These processes contribute differentially to plant growth and final yield depending on the severity of stress and the nature of limiting conditions. For instance, nitrogen balance may be considered a secondary process under water-deficit conditions.(Weiss et al., 2020)

Moreover, climate change represents one of the most complex contemporary global challenges, having led to temperature shifts, heat waves, altered weather patterns, and rainfall uncertainty, all of which have adversely affected agricultural sustainability and contributed to declining crop yields(Kumawat et al., 2023a)

3.2. Spectral Indices for Crop Assessment

3.2.1. Vegetation index

vegetation index are mathematical combinations or ratios of spectral bands, primarily red, green, and infrared, that are used to establish functional correlations between crop features and remote sensing observations". "The interaction of solar radiation with crop photosynthesis greatly influences vegetation indices, which are indicative of the dynamics of biophysical parameters connected to crop state. However, at early stages of crop development, the impacts of soil reflectance have an impact on the values of various vegetation indices used to detect crop stress". Vegetation indices are spectral indices that describe the volume, density, health, and vitality of vegetation. The normalized difference vegetation index (NDVI) scale ranges from -1 to +1, and it is favorably associated to a substantial amount of high-quality vegetation (the larger value of the NDVI, the more abundant and healthier the vegetation). Several studies reveled that the application of NDVI and other spectral indices for measuring the leaf chlorophyll content and relative water content of crop plants, which can provide the data concerning the physiological status of a plant. Daughtry et al. classified vegetation indices into two categories: first, intrinsic vegetation indices that include the ratios of two or more bands in the visible and near-infrared wavelengths; these indices are sensitive to soil **background reflectance and can be difficult to interpret at low Leaf Area Index (LAI) . The soil-line VIs is the second type, and they employ the information from a regression line in the NIR-Red space to lessen the effect of the soil on canopy reflectance. Some of vegetation index and their potential uses in precision agriculture showed in Table 2.(Kumawat et al., 2023b)**

3.2.2. Normalized Difference Vegetation Index (NDVI)

NDVI is the most widely used and important spectral index, calculated as follows:

$$NDVI = \frac{NIR - RED}{NIR + RED} \dots\dots\dots\dots\dots\dots. (04)$$ (Mahmood & Al-Rawe, 2023)

where NIR denotes reflectance in the near-infrared band and RED denotes reflectance in the red band.(Sishodia et al., 2020b)

NDVI values range from −1 to +1, where positive values indicate increasing greenness (indicative of leaf area and vigor), and negative values correspond to non-vegetated surfaces such as urban areas, bare soil, and water bodies.(Sishodia et al., 2020b) Specifically: values near −1 indicate water surfaces; values between −0.1 and 0.1 correspond to arid areas; values between 0.2 and 0.4 represent shrublands and grasslands; and values approaching 1 indicate dense forest.(Mahmood & Al-Rawe, 2023)

However, NDVI exhibits certain limitations:(Sishodia et al., 2020b)

- Sensitivity to confounding effects from soil background, atmospheric conditions, cloud cover, and canopy shadows.
- Loss of sensitivity beyond a saturation threshold, particularly under dense vegetation canopy conditions.

Table 3. Spectral Vegetation Indices in Precision Agriculture (Kumawat et al., 2023a)

Index	Formula	Applications in agriculture
Normalized Difference Vegetation Index (NDVI)	(R830 – R670)/(R830 + R670)	Physiology [68] Plant health, Yield [69]
Normalized difference red edge index (NDRE)	(RNIR−Rred edge)/(RNIR+Rred edge)	Plant stress detection [70], Nitrogen and water status [71]
Green Normalized difference vegetation index (GNDVI)	(R750-R550) / (R750 + R550)	Chlorophyll [72]
Ratio index (RI-1 dB)	R735/R720	Chlorophyll [73]
Photochemical Reflectance Index (PRI)	(R531 - R570)/(R531+R570)	Physiology Photosynthesis [74]
Normalized Photochemical Reflectance Index (PRInorm)	PRI / [RDVI×(R700/R670)]	Chlorophyll fluorescence Stomatal conductance [75,76]
Plant Senescence Reflectance Index (PSRI)	(R678 - R500)/R750	Chlorophyll/Carotenoids Senescence [77]
Modified Chlorophyll Absorption in Reflectance Index (MCARI)	[(R700 - R670) - 0.2 * (R700 - R550)]* (R700/R670)	Green leaf area index Chlorophyll [78]
Red edge Chlorophyll index (CI red-edge1)	[(R750-R800)/(R695-R740)]-1	Chlorophyll [79]
Normalized difference water index (NDWI)	(R857 – R1241)/(R857 + R1241)	Leaf water potential [80]
Green index (GI)	R554/R677	Crop greenness and stress identification [81]
Modified normalized difference vegetation index (mNDVI)	(R800 – R680)/(R800 + R680 – 2R445)	leaf pigment content [82]
Triangular vegetation index (TVI)	0.5 [120(R750 – R550) – 200(R670 -R550)]	green leaf area index and canopy chlorophyll density [83]
water index (WI)	R970/R900	Leaf water potential [84] Yield of wheat under water stress [85]
normalized water index-1 (NWI-1)	(R970−R900)/(R970+R900)	Grain Yield & biomass yield of wheat under water stress [85] LAI[86]
normalized water index-2 (NWI-2)	=(R970−R850)/(R970+R850),	Yield [85]
normalized water index-3 (NWI-3)	(R970−R920)/(R970+R920)	Yield [85]
Enhanced Vegetation Index (EVI)	2.5*(RNIR−RRed)/ (RNIR+6RRed−7.5RBlue+1)	Disease [87] yield [69]
Plant Pigment ratio (PPR)	(Rgreen − Rblue)/(Rgreen + Rblue)	Chlorophyll [88]
photosynthetic vigour ratio	(R550−R650)/(R550+R650)	Identification of healthy and stressed plants
Gitelson and Merzlyak index (GMI)	R750/R550	Chlorophyll [89]
Carter index 1 (Ctr1)	R760/R695	Stress [90]
Copper Stress Vegetation Index (CSVI)	R550/R850 ×R700/R850	Copper content [91]
New Vegetation Heavy Metal Pollution Index (VHMPI)	DCR505 - DCR640/ DCR690 -DCR730	Copper content [92]

3.2.3. Other Key Spectral Indices (SAVI, NDWI)

Soil-Adjusted Vegetation Index (SAVI):

$$SAVI = \frac{(1+L)(NIR - RED)}{NIR + RED + L} \dots\dots\dots\dots\dots\dots.(05)(\text{Sishodia et al., 2020b})$$

where L is a soil adjustment factor (typically ranging between 0.5 and 1.0). This index introduces a correction factor to minimize soil background effects, yielding more reliable results in environments with sparse vegetation cover. SAVI has demonstrated high accuracy in retrieving chlorophyll content in black-eyed pea crops.(Sishodia et al., 2020b)

Normalized Difference Water Index (NDWI): Used to estimate water content in vegetation and water bodies. It has been applied to assess land suitability for vegetable cultivation in India.(J. Zhang, 2025)

Additional important indices:

- **NDRE (Normalized Difference Red Edge):** Outperforms NDVI in estimating nutrient status and leaf area index under dense canopy conditions.
- **EVI (Enhanced Vegetation Index):** Incorporates the blue band to correct for atmospheric effects.

- **OSAVI (Optimized Soil-Adjusted Vegetation Index):** Substitutes the conventional red band with the red-edge band.
- **GNDVI (Green NDVI):** Replaces the red band with the green band to mitigate NDVI saturation.
- **CWSI (Crop Water Stress Index):** A widely used index for estimating irrigation water demand.(Sishodia et al., 2020b)

4. Applications of GIS and Remote Sensing in Precision Agriculture

4.1. Crop Area Estimation and Classification

Multispectral satellite data enable the classification of imagery into land cover maps that identify major crop types and other land uses, achieving classification accuracies exceeding 90% for principal crops.(Sangeetha et al., 2024) Accurate classification requires spatial resolution commensurate with field size, particularly for smallholder farms — in Africa, approximately 25% of fields are smaller than 0.5 acres.(Weiss et al., 2020)

Hassan et al. employed UAV imagery, GIS tools, and deep learning to assess crops across more than 40 acres of rice paddies in Pakistan, where the deep learning model detected rice plants with an accuracy of 99%.(J. Zhang, 2025)

Machine learning and deep learning algorithms are increasingly employed to improve classification outcomes, including decision trees, support vector machines (SVM), neural networks, and ensemble methods such as Random Forest and XGBoost.(S. Zhang et al., 2025)

4.2. Crop Monitoring and Stress Detection

Time-series spectral indices derived from satellite imagery enable the tracking of vegetation vigor and phenological stages throughout the growing season.(Sangeetha et al., 2024) Key applications include:

4.2.1Water Stress Detection:

Remote sensing and GIS have become increasingly important for the detection, assessment, and management of agricultural drought, as they provide updated information at diverse spatial and temporal scales that are difficult to obtain through conventional methods.(Kumawat et al., 2023a) Indices such as NDWI and the Photochemical Reflectance Index (PRI) can be used to monitor crop water status.(S. Zhang et al., 2025)

4.2.2Pest and Disease Detection:

Studies have demonstrated that hyperspectral imaging can be used to diagnose pest and disease infestations in crops. Machine learning techniques combined with spectral indices derived from UAV imagery have achieved early disease detection accuracies of up to 96%.(Kumawat et al., 2023a) Random Forest classifiers achieved a 97.3% accuracy in detecting Fusarium wilt in banana using five-band data.(S. Zhang et al., 2025)

4.2.3Growth and Vigor Monitoring: Key indicators that characterize the physiological status of crops include: Leaf Area Index (LAI), chlorophyll content, seedling emergence rate, above-ground biomass, and vegetation fractional cover.(S. Zhang et al., 2025)

4.3. Yield Estimation

Yield estimation have a critical importance in precision agriculture as it enables farmers to accurately forecast potential production. Yield prediction using remote sensing has generally been based on empirical-statistical relationships between vegetation indices and observed yields.(Kumawat et al., 2023a)

The principal methodological approaches include:(Weiss et al., 2020)

- ✓ **Empirical Approach:** Establishes direct relationships between vegetation indices (e.g., NDVI) and observed yield data.
- ✓ **Mechanistic Approach:** Integrates biophysical parameters derived from remote sensing (e.g., LAI) with crop growth simulation models such as DSSAT, WOFOST, and STICS.

An alternative approach combines remote sensing data with meteorological observations within crop growth models, enabling within-season yield forecasts with error margins of 8–15% at regional scales.(Sangeetha et al., 2024)

Machine learning techniques such as Partial Least Squares Regression (PLSR) have achieved a coefficient of determination of 0.753 for maize yield prediction, while the AlexNet model integrating multispectral imagery and weather data achieved an RMSE of 0.859 for rice yield prediction.(S. Zhang et al., 2025)

4.4. Water Resource Management

Remote sensing plays a pivotal role in agricultural water resource management through several key dimensions:

- ✓ **Evapotranspiration (ET) Estimation:** Remote sensing products across the optical, thermal, and microwave domains are used to develop and validate multiple indices and techniques for precision water management.(Sishodia et al., 2020b) Principal methods include: surface energy balance approaches (e.g., SEBAL and METRIC), crop coefficient methods, and the Penman-Monteith approach.(Sishodia et al., 2020b)
- ✓ **Soil Moisture Estimation:** The triangle method (LST-VI) exploits the physical relationship between land surface temperature and vegetation cover to estimate soil moisture. The OPTRAM model was also developed, which substitutes land surface temperature with shortwave infrared-transformed reflectance.(Sishodia et al., 2020b)
- ✓ **Variable-Rate Irrigation:** Remote sensing data can assist in identifying within-field variability and implementing variable-rate irrigation with common irrigation systems such as center pivots. Variable-rate application can mitigate water stress arising from both excessively wet and dry conditions, thereby achieving uniform high productivity across the field while reducing water and nutrient losses.(Sishodia et al., 2020b)

In practical terms, a Greek study by Filintas demonstrated that combining TDR sensors with GIS modeling supports the efficient use of water and improved crop productivity in arid regions. Limited drip irrigation during critical growth stages increased coriander seed yield from 422.37 kg/ha to 1203.47 kg/ha.(J. Zhang, 2025).

CHAPTER II

The Conceptual Framework of Geographic Information Systems (GIS)

1.Geographic Information Systems (GIS)

1.1. Definition and Historical Development of GIS

1.1.1. Definition of GIS:

computer-based system that support capture, management, manipulation, analysis, modeling, and display of spatially referenced data that provides planning, management, development and humanitarian solutions(Omol-Lecturer, 2019)

1.1.2. History of Geographic Information System:

GIS is an extension of cartography and the concept began through trying to understand cholera outbreaks in Europe during the 19th century. In 1854 John Snow discovered that London cholera outbreaks were concentrated around a water pump, by marking outbreaks on a map. This was the beginning of spatial analysis. GIS has since evolved from paper maps to the concept of layers, through the use of transparencies, and now to computers. Roger Tomlinson pioneered GIS through his role in developing the Canada Geographic Information System (CGIS). The CGIS aimed to integrate natural resource data to create a Canadian national land use management program. The improvement in computers and the advantages of GIS lead to commercialization of software in the 1980s. Today GIS gives people the ability to solve real world problems by creating their own maps by combining different sets of data relevant to each problem.(Wilson et al., n.d.)

1.2. Components of a Geographic Information System

A Geographic Information System (GIS) is composed of five major components:

- ✓ **Hardware:** Modern GIS platforms operate across a wide range of computing environments, from high-capacity data servers to networked desktop computers or standalone workstations.
- ✓ **Software:** GIS software provides the tools and functionalities required to store, manage, analyze, and visualize spatial data. Its key components include tools for data capture and manipulation, database management systems, spatial query and analysis tools, as well as user-friendly graphical interfaces.
- ✓ **Data:** Data constitute the most critical component of any GIS. This includes both spatial (geographic) data and their associated attribute (tabular) data, which can be generated internally or obtained from external data providers(laouini &nine, 2024)
- ✓ **Users:**

As a Geographic Information System (GIS) is fundamentally a tool, its true value is realized through its use—therefore, through its users. GIS serves a broad spectrum of users, ranging from specialists who design and maintain the systems to professionals who integrate geographic information into their daily work.

✓ **Methods:**

The implementation and effective operation of a GIS require adherence to a set of structured rules and procedures, which vary according to the specific context and organizational framework

1.3. Types of Spatial Data: Raster and Vector

1.3.1 Geographic Data:

Information layers can be represented in the form of geographic data, which describe the spatial characteristics and geometry of features located in space. A distinction is commonly made between **raster data** and **vector data**.

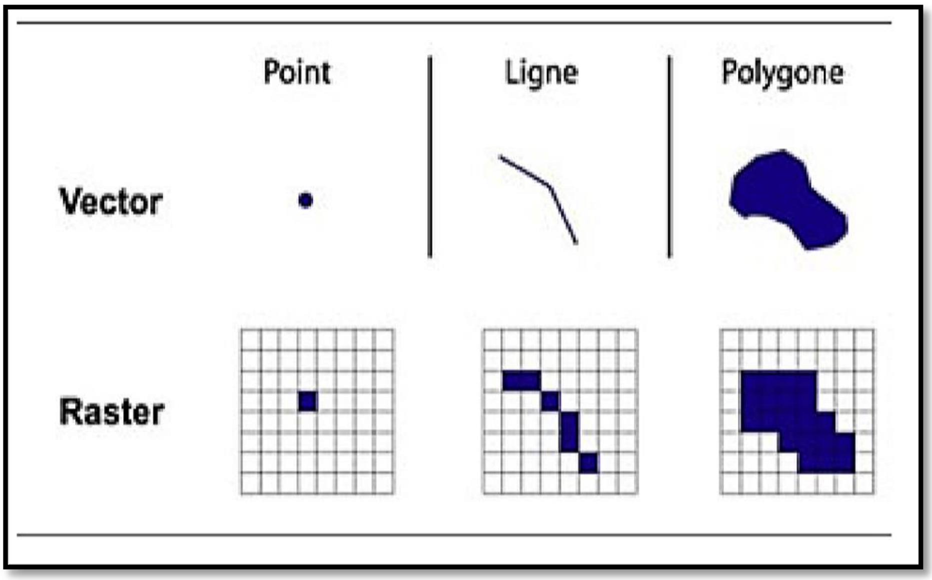

Figure 05: Types of Geographic Data in a GIS.

1.3.2Vector Data:

In this data model, a point defined by its coordinates serves as the fundamental carrier of geometric information. Lines and polygons are represented as structured sequences of characteristic points. Vector data are most commonly generated through manual or semi-automated digitization processes. In general, vector datasets distinguish between point, line, and polygon features, which are typically organized and managed as separate layers (laouini &nine; 2024)

1.3.3 Raster Data:

Raster data are fundamentally based on the pixel (picture element) as their primary unit. They are typically derived either from the digitization of maps or from digital imagery such as satellite images. Pixels are arranged in a regular grid structure within the raster. Linear and areal features can only be represented through contiguous arrangements of individual pixels. Consequently, objects are depicted in an approximate manner, and the spatial resolution—determined by pixel size—directly influences the accuracy of the representation (laouini &nine; 2024)

1.4 Core Spatial Analysis Functions

A Geographic Information System (GIS) stores information about the real world in the form of thematic layers that can be interconnected through their geographic relationships. This concept, both simple and powerful, has proven highly effective in addressing a wide range of practical problems

Geographic Referencing:

Geographic information may include either an explicit spatial reference (such as latitude and longitude or a national coordinate grid) or an implicit reference (such as an address, postal code, or road name). Geocoding—an automated process—is used to convert implicit references into explicit spatial coordinates, thereby enabling the precise location of objects and events on the Earth's surface for analytical purposes (laouini &nine; 2024)

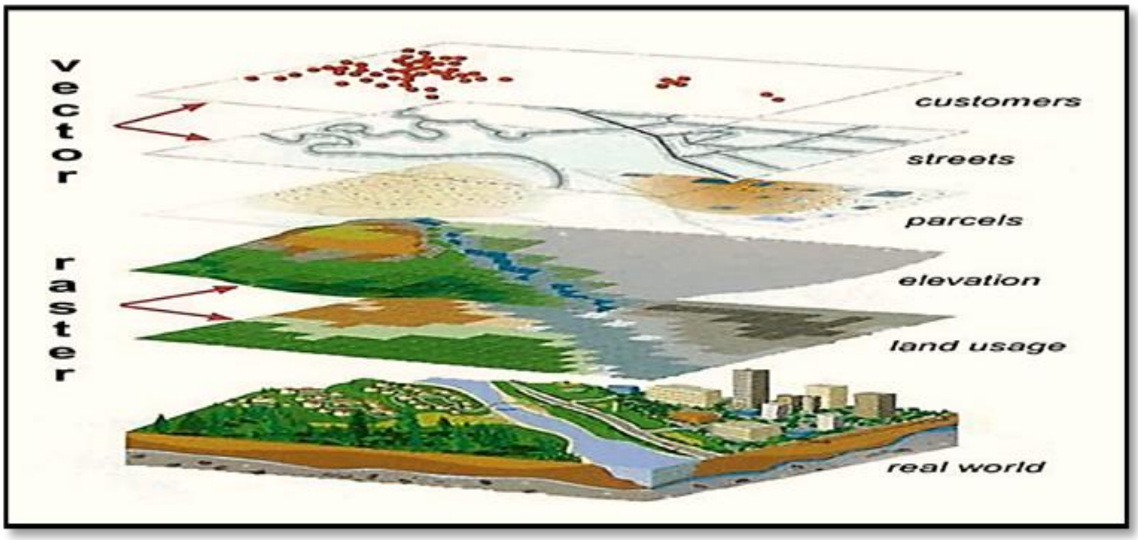

Figure 06: Representation of Thematic Layers

1.5 Q GIS

1. Overview

- QGIS is an open-source Geographic Information System (GIS) software, initiated in 2002 as a free and viable alternative to proprietary software such as ArcGIS.
- It supports the visualization and analysis of spatial data in both 2D and 3D environments.
- **Definition of Q GIS:**
- QGIS is an Open-Source Geographic Information System. This means QGIS is free software, making GIS available to anyone with access to a computer.

2. Key Features

- **Data Visualization**: Supports multiple data formats (Shapefile, GeoPackage, GeoTIFF) and web services (WMS, WFS).
- **Data Editing**: Provides advanced digitizing tools and a Georeferencer module for coordinate registration.
- **Spatial Analysis**: Includes statistical tools, geoprocessing functions, and a raster calculator.
- **Map Output**: Features an integrated Print Layout with standard map elements (north arrow, scale bar).

3. Plugin System

- Divided into core plugins (e.g., DB Manager, Georeferencer, Zonal Statistics) and external plugins available through the Python repository.
- The Processing Framework integrates algorithms from GDAL, SAGA, GRASS, and R.

4. Python Interface and Automation

- Offers a Python Console with code completion and syntax highlighting.
- Provides the PyQGIS API for plugin development and task automation.
- Supports batch processing and graphical modeling.

5. Recent Release: QGIS 4.0 "Norrköping" (March 2026)

- Migration from Qt5 to Qt6, enhancing performance and security.
- Updated user interface with a new welcome screen.
- Over 100 new features, requiring existing plugins to be updated for compatibility.

6. Applications in Scientific Research

- Widely used for satellite image processing (e.g., Sentinel-2), vegetation cover analysis (e.g., NDVI calculation), and spatial data management. (QGIS Project, 2024).

CHAPTER III

STUDY OF THE REGION

1.Geographical Location

The province of El Oued, one of the most important cities at the national level, is located in the vast East Southeastern region and occupies a large area of 35,752 square kilometers, representing 1.5% of the total territory of the Algerian Republic. The province covers an area of 35,752 km² (i.e., 1.5% of the national territory), and its population as of the end of 2021 is estimated at 716,905 inhabitants, with a population density of 20.05 inhabitants per km². The province of El Oued is situated in the southeast of the country and shares the following borders:

- **To the north:** Khenchela Province
- **To the northeast:** Tébessa Province
- **To the northwest:** El M'Ghair Province
- **To the west:** Touggourt Province
- **To the southwest:** Ouargla Province
- **To the east:** The Republic of Tunisia (with a border strip of 260 km)

2. Study area

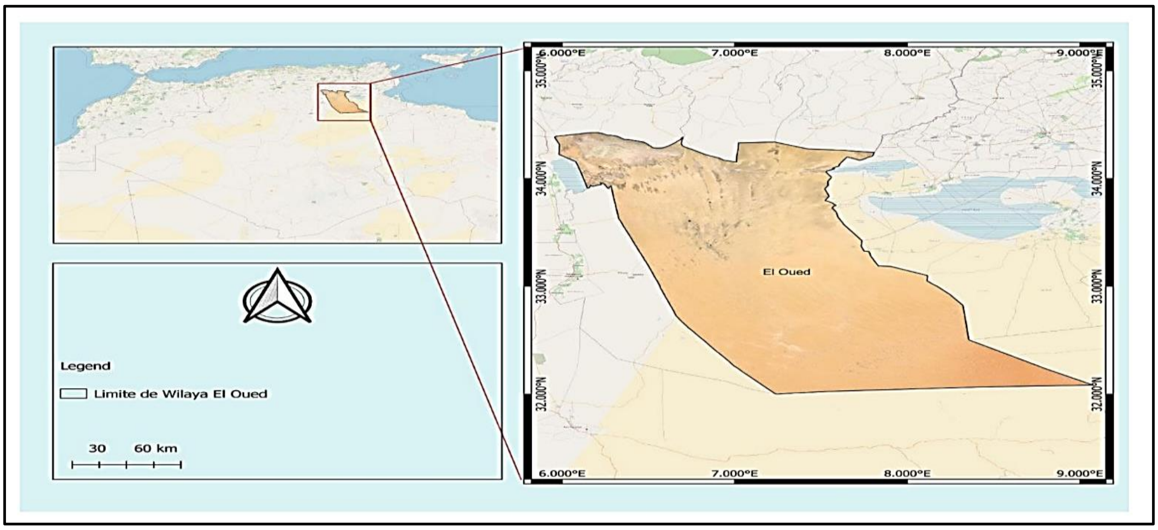

Figure 07: Geographic location of the El Oued region (Produced by QGIS)

3.1. Topographic Nature of the Study Area

El Oued region, also referred to as the Lower Sahara region due to its low elevation, is located in the southeastern part of the country. The highest point is at an elevation of 125 meters in the municipality of Bayadha (Soualah), while the lowest point is at 29 meters in the municipality of Réguiba (Foulia). The average elevation of the region is 80 meters, and it exhibits a notable decrease from south to north, reaching 25 meters below sea level in the Chott area, which occupies the bottom of the vast Lower Sahara basin.

3.2. Terrain Slope

The general dip of the study area is oriented south-to-north, with a very low average slope (at best on the order of 0.002 m/m to 0.003 m/m), along with irregularities related to the presence of dunes. **(cité par, TOUATI, ABBIDI ,2018).**

Table 4: Average altitude of the different municipalities of the El Oued (Cité par, TOUATI, ABBIDI ,2018).

N°	The commune	Mean Altitude (m)	N°	The commune	Mean altitude (m)
01	Hassi Khalifa	77	10	Sidi Aoun	54
02	El-Ogla	91	11	Trifaoui	81
03	Mouih Ouansa	91	12	Magrane	60
04	El-Oued	77	13	Ourmes	85
05	Robbah	93	14	Kouinine	75
06	Oued Allenda	83	15	Reguiba	57
07	Bayadha	90	16	Taghzout	78.5
08	Nakhla	85	17	Debila	62
09	Guemar	64	18	Hassani Abdelkrim	66

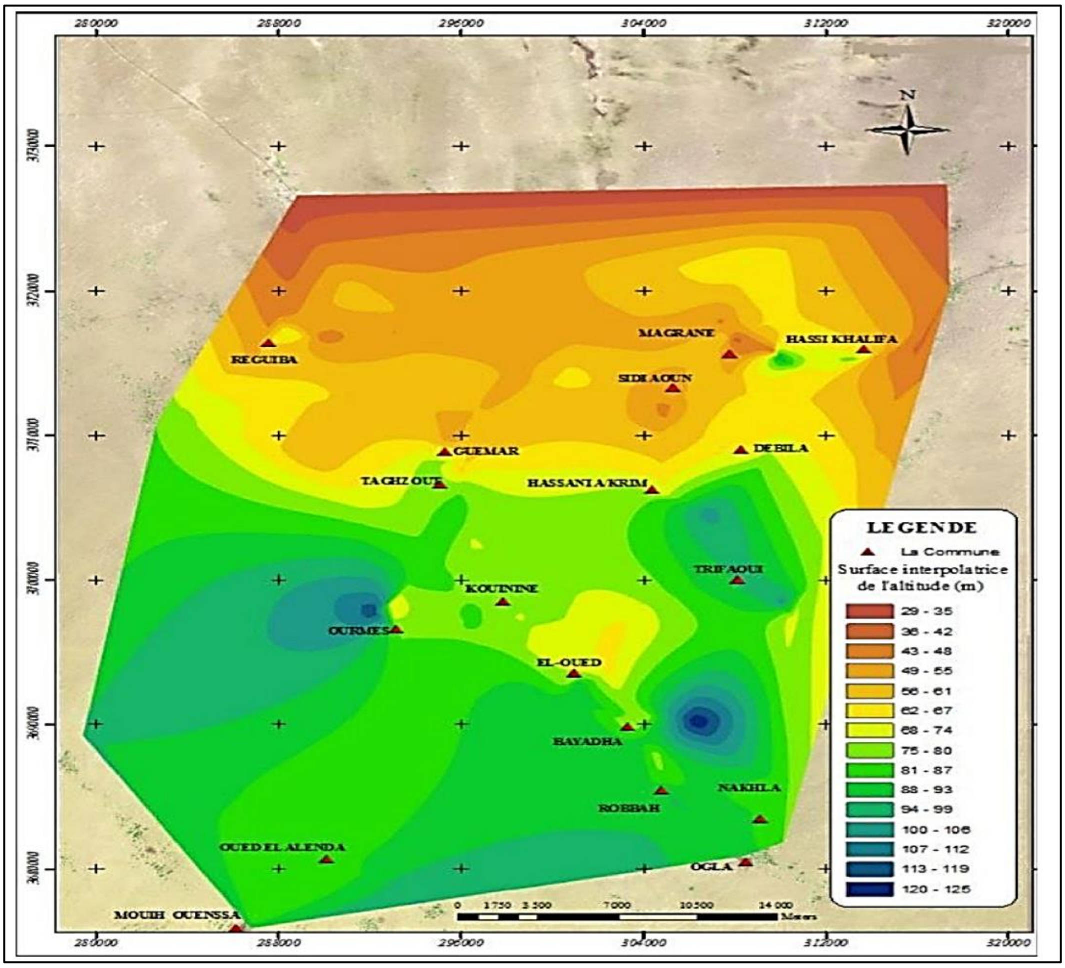

Figure 08: Topographic map of the El Oued valley

4. Climate

The study of the climate of the El Oued region was conducted for the period (2013–2023), based on data collected from the National Meteorological Office of Gamar.

4.1. Temperature

Table 01 shows that the mean annual temperature recorded in El Oued is 25°C. The minimum temperature is recorded in January, at 9°C, and the highest temperature is recorded in July, at 45°C. The number of months with temperatures exceeding 30°C ranges from 4 to 5 months, depending on the year.

Table 5: Average monthly temperatures of the El Oued region during the period 2013–2023 Source (ONM)

Months	Jan	Feb	Mar	Apr	May	Jun	Jul	Aug	Sep	Oct	Nov	Dec	Yearly average
T max	18	18	22	23	33	44	45	43	37	29	24	15	29.3
T min	9	11	16	20	23	26	30	32	29	26	16	11	20.8
T mean	13.5	14.5	19	21.5	28	35	37.5	37.5	33	27.5	20	13	25

4.2 Relative Humidity

Table 6: Average monthly humidity of the El Oued region during the period 2013–2023 Source (ONM)

Months	Jan	Feb	Mar	Apr	May	Jun	Jul	Aug	Sep	Oct	Nov	Dec	Total
H(%)	56.9	49.4	41.6	36.9	33	30.5	26	33	39.4	47	55.1	65.5	42.9

4.3. Wind

The winds are characterized by an average speed of 3.07 m/s. They blow throughout the year with varying speeds depending on the season

Table 7 : Average monthly wind speed of the El Oued region during the period 2013–2023

Months	Jan	Feb	Mar	Apr	May	Jun	Jul	Aug	Sep	Oct	Nov	Dec	Total
Wind speed (m/s)	2.5	2.7	3.5	3.7	3.7	3.8	3.2	3.3	3.3	2.44	2.6	2.1	3.07

4.4 Rainfall

Rainfall is scarce and irregular. The highest rainfall amounts are recorded in April, with 4.2 mm. The annual cumulative precipitation is 24.4 mm.

Table 8: Average monthly precipitation in the El Oued region during the 2013–2023 period

Months	Jan	Feb	Mar	Apr	May	Jun	Jul	Aug	Sep	Oct	Nov	Dec	Total
Rainfall (mm)	1.3	2.6	2.4	4.2	1.33	0.2	0	0.7	2.6	2.2	3.3	3.6	24.4

5.1 Bagnouls and Gaussen ombrothermic diagram:

To provide a climatic synthesis of the study area, we established the Bagnouls and Gaussen ombrothermic diagram (**Figure 9)** and the Emberger climagram (**Figure 10**).

The Bagnouls and Gaussen ombrothermic diagram is a graphical method used to define the dry and wet periods of the year. For the El Oued region, and based on the average monthly precipitation and temperature data calculated over an 11-year period, we observe that the dry period extends throughout the entire year (**Figure 9).**

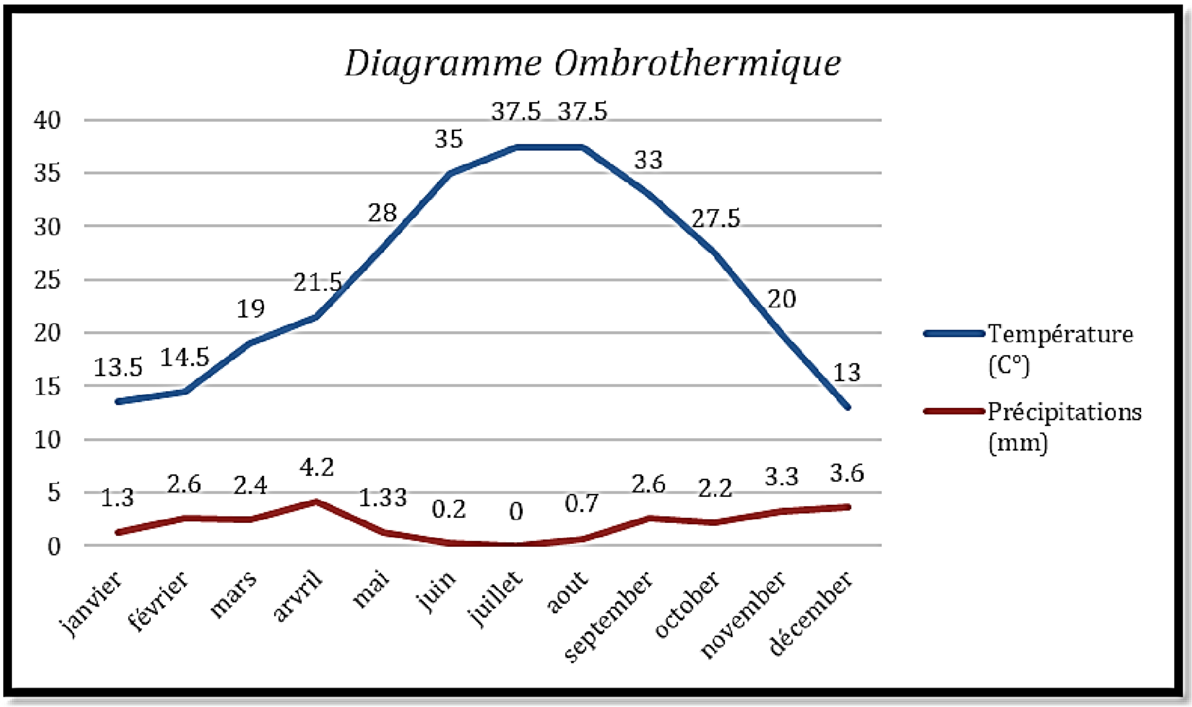

Figure 09: Bagnouls and Gaussen ombrothermic diagram

5.2 Emberger climagram

This climagram allows, through Emberger's pluviometric quotient (Q2) specific to the Mediterranean climate, to place a study area within a bioclimatic stage. Emberger's pluviometric quotient is calculated using the following formula:

$$Q2 = 3.43 \times P / (M - m) = 3.43 \times 24.4 / (45 - 9) = 2.32$$

Where:

- **Q2:** Emberger's pluviometric quotient.
- **P:** Annual precipitation (mm).
- **M:** Mean maximum temperature of the warmest month.
- **m:** Mean minimum temperature of the coldest month.
- **3.43:** Stewart coefficient established for Algeria.

Thus, these values allow us to classify the El Oued region, according to Emberger's climagram, within the Saharan bioclimatic stage with mild winters (**Figure 10)**

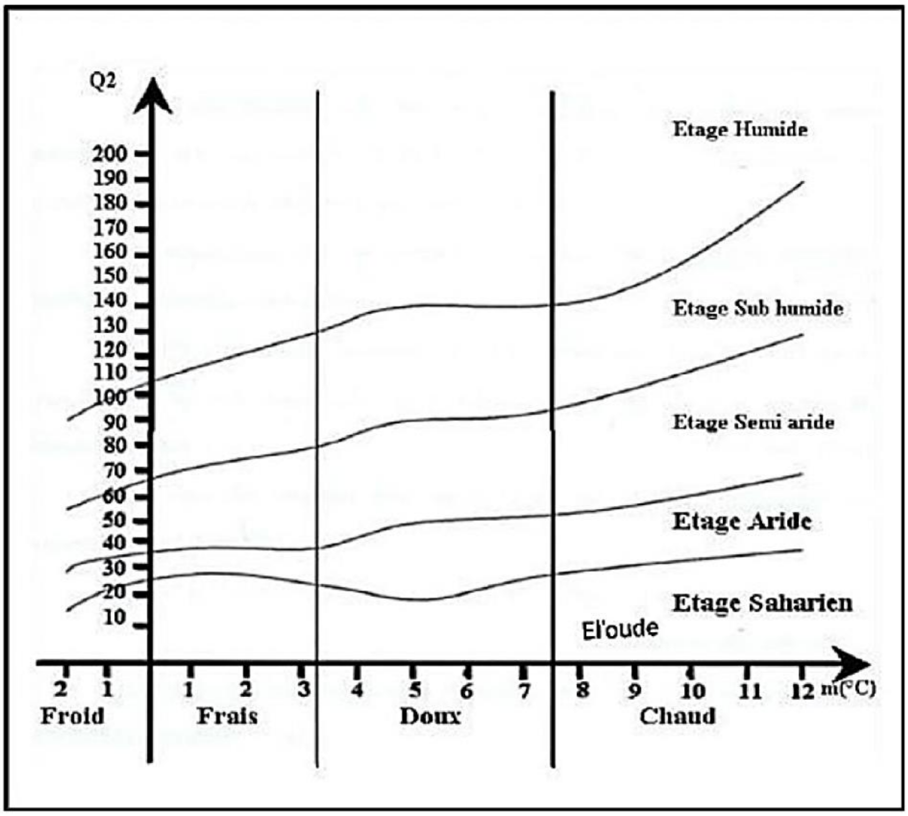

Figure 10: Location of the El Oued region on the climagram

6. Natural characteristics

6.1. Natural zone

The wilaya of El Oued is located in the northeastern part of the northern Sahara. The terrain lies significantly below sea level along the El Oued–Mugheir axis (Shat zone), ranging from 75 m to 6 m below sea level.

The major geographical units characterizing the natural landscape of the wilaya are divided into two regions:

- **Ridges and depressions in the north:** This area extends around Malgheig and Shat Marwan. It is primarily known for palm cultivation in the north and for pasture farms in the northern and western parts.
- **Eastern lowlands in the south:** The proximity of the shallow aquifer in this area has enabled palm cultivation without regulated irrigation (the *Ghout* technique). In recent years, the region has witnessed significant development in field crops and greenhouses, particularly tomatoes and potatoes (Monograph of El Oued Wilaya).

6.2. Geographical zone

Throughout the entire wilaya, deposits have formed over all major topographic highs, where geological and gypsiferous mounds converge in the east. These mounds are all part of the ninth desert basin. The wilaya is situated in a stable zone, where the risk of earthquakes is very low or nonexistent.

Moreover, the main rock types found across the wilaya, particularly within these mounds, are sedimentary rocks (of chemical origin), such as salt crusts and sand.

7. Water resource potential of the wilaya

The El Oued wilaya contains large quantities of groundwater stored in subsurface reservoirs that are part of the northern Sahara aquifer system. These water reservoirs, referred to as groundwater aquifers, are considered fossil aquifers because their natural recharge is negligible compared to the current rates of water withdrawal (Monograph of El Oued Wilaya).

7.1. The groundwater aquifers found in this region are as follows

- **Phreatic aquifer:** This groundwater is distributed throughout the valley and is captured by traditional shallow wells within an endorheic basin (closed basin with no outlet).
- **Downstream aquifers:** These reservoirs are located in this area at depths between 200 and 500 m. The static water level ranges from 10 to 60 m, and water salinity ranges from 3 to 6 g/L.
- **Continental Albian Aquifer:** The Albian Aquifer is little exploited due to its depth and high extraction cost. The extraction depth of this aquifer can reach 1900 m, providing a flow rate of up to 200 L/s at a temperature exceeding 60 °C and a dry residue of 2–3 mg/L.

7.2. Surface water resources

The wilaya of El Oued is part of the lower desert basin, characterized by the virtual absence of any relief. The extensive, very flat area with depressions across the entire northern part of the wilaya serves as an outlet for rainwater, which is drained by the border basins to the north and conveyed by the valleys of Al-Rutam, Al-Kharf, and Wadi Yatl, all of which terminate in the Shatt region (Monograph of El Oued Wilaya).

8 . Social, cultural and economic activity

The economy of the wilaya depends primarily on agriculture and pastoralism. The total utilized agricultural area amounts to 86,270 hectares (2020–2021). Below are some of the most important products:

- **Palm cultivation:** 1,216,669 quintals of dates on an area of 15,374 hectares.
- **Field crops:** Total production of 19,257,425 quintals, including potatoes (12,938,925 quintals) and tomatoes (3,292,230 quintals) for the 2020–2021 agricultural season.

9. General type of agriculture

Potato cultivation is considered the most widespread, occupying an area of 43,970 hectares, with an estimated production of 12,896,400 quintals. Meanwhile, date palm cultivation produces 3.8 million palm trees over an area of 37,000 hectares, of which 2.4 million are of the highest-quality variety (Deglet Nour), making the province the second-largest producer of this fruit in the country.

Peanut cultivation, a thriving experience in the wilaya, has also gained ground due to growing interest from farmers, reaching an area of 1,670 hectares spread across six municipalities, producing over 50,000 quintals, accounting for 47% of national production. The El Oued province also ranks at the top of tobacco-producing regions, with a production of 40,000 quintals representing 41% of national output, harvested from a total area of 1,680 hectares mainly located in the Guimar and Rigueba regions (northern part of the wilaya). (DSA)

According to the Chamber of Agriculture of El Oued, the sector has developed so significantly that by 2013 the wilaya had become the leading potato-producing region in Algeria, accounting for 24% of the 5 million tonnes harvested nationwide.

SECOND PART

Applied section

CHAPTER I: Study of The Barley Crop using NDVI

Introduction generale:

Monitoring crop growth and tracking changes in vegetation cover are among the key applications of remote sensing and geographic information systems (GIS) in agriculture. These tools provide accurate spatial and temporal information on plant health and green biomass density without the need for continuous field interventions, thereby saving time and effort. Among the most widely used spectral indices in this context is the **Normalized Difference Vegetation Index (NDVI)**, which serves as an effective indicator for assessing plant photosynthetic activity and estimating biomass.

The objective of this study is to prove that remote sensing and GIS (specifically the NDVI index) can deliver precise and trustworthy results applicable to vegetation cover prediction, crop growth monitoring, and agricultural decision support, by investigating barley in the Debila area and conducting a case study of the Oued Righ region over the past decade.

1.1 Study Site

The study was conducted in an experimental field cultivated with barley (*Hordeum vulgare* L.), located in the municipality of Debila, El Oued Province, southeastern Algeria. The geographic coordinates of the field were recorded using a Global Positioning System (GPS) at the following point: 33.5231525° N, 6.9810004° E.

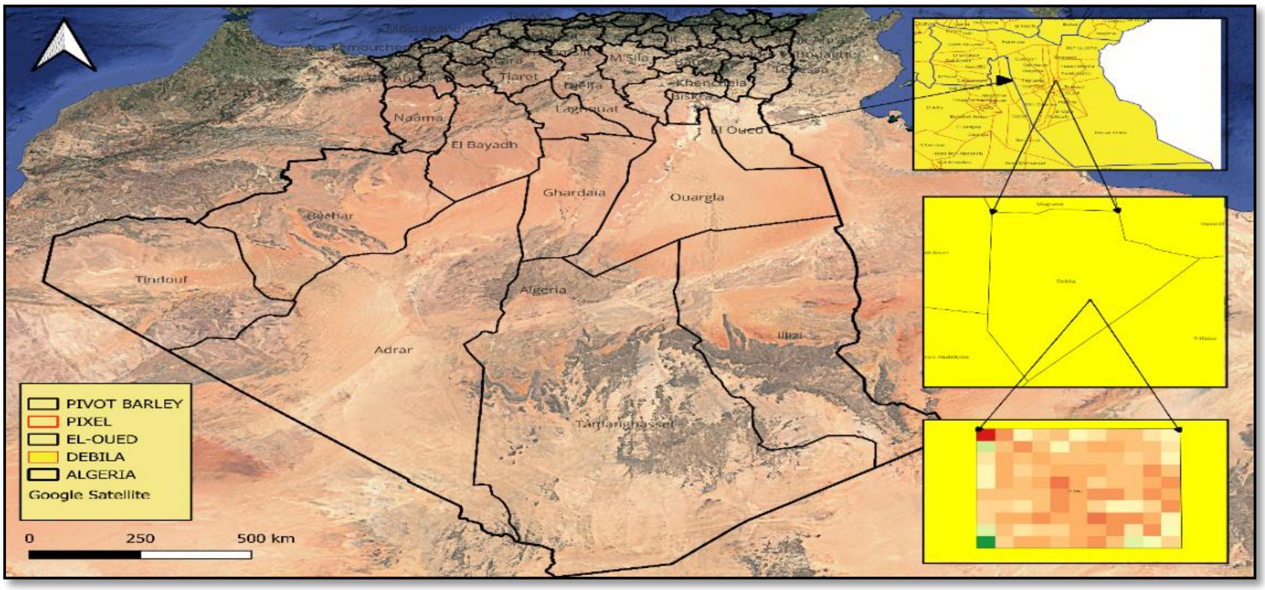

Figure 11: Barley Field Location

1.2 Crop Material

The field was was seeded late on February 26, 2026, using barley seeds. The irrigation system applied was the traditional center-pivot irrigation system.

Figure 12: Barley Pivot

1.3 Measurement Equipment

Sample pixel: A square area measuring 10 m × 10 m (100 m²) within the field was designated as the reference ground pixel, in accordance with the spatial resolution of the Sentinel satellite, which is 10 meters. The coordinates of this pixel were recorded using the Global Positioning System (GPS) as follows:

Table 9 : Pixel Coordinates

Pix coord	Longitude	Latitude
station 1	6.98079467	33.523139
station 2	6.98090198	33.523141
station 3	6.98079676	33.52305
station 4	6.98090408	33.523051

2. Method:

2.1 Field Sampling

A **10 m × 10 m pixel** was selected within the field to serve as the basic monitoring unit. Within this pixel, samples were taken **randomly** during each field visit to avoid spatial bias. The sampling locations were marked with temporary stickes during every visit to ensure approximately the same positions were revisited.

2.2 Plant Height Measurement

During each weekly visit, **10 plants** were randomly selected within the pixel. The height of each plant was measured using the graduated ruler, from the soil surface to the tip of the tallest leaf (or the spike at the maturity stage). The values were recorded, and then the **mean plant height (in centimeters)** was calculated for each week.

Evolution of average plant height:

Table 10: Evolution of average plant height:

Date	Plant Height(cm)
26_02	0
08_03	3
18_03	10
28_03	18
02_04	21
07_04	27

09_04	35
17_04	50
19_04	55
27_04	66
02_05	63
19_05	61
22_05	59

Figure 13: Barly 08/03/2026

Figure 14: Barley 18/03/2026

Figure 15: Barley 06/04/2026

Figure 16: Barley 12/05/2026

2.3. Growth Curve Plotting Using Excel Software

After completing the 12 weekly plant height measurements, the data were entered into Microsoft Excel. The worksheet was organized into two main columns:

- **X-axis (abscissa):** Weeks after sowing, ranging from week 1 (sowing date: February 26, 2026) to week 12.
- **Y-axis (ordinate):** Mean plant height (in centimeters) measured for each week.

A **"Line with Markers"** chart type was selected. The X-axis was set to represent the weekly visits (Week 1, 2, 3, …, 12), and the Y-axis was set to represent the mean plant height (cm). After generating the chart, the following labels were added: chart title **"Growth Curve of Barley Under Center-Pivot Irrigation"**, X-axis title **"Week After Sowing (week)"**, and

Y-axis title **"Mean Plant Height (cm)"**. In this way, a growth curve illustrating the vegetative development of barley throughout the study period was obtained.

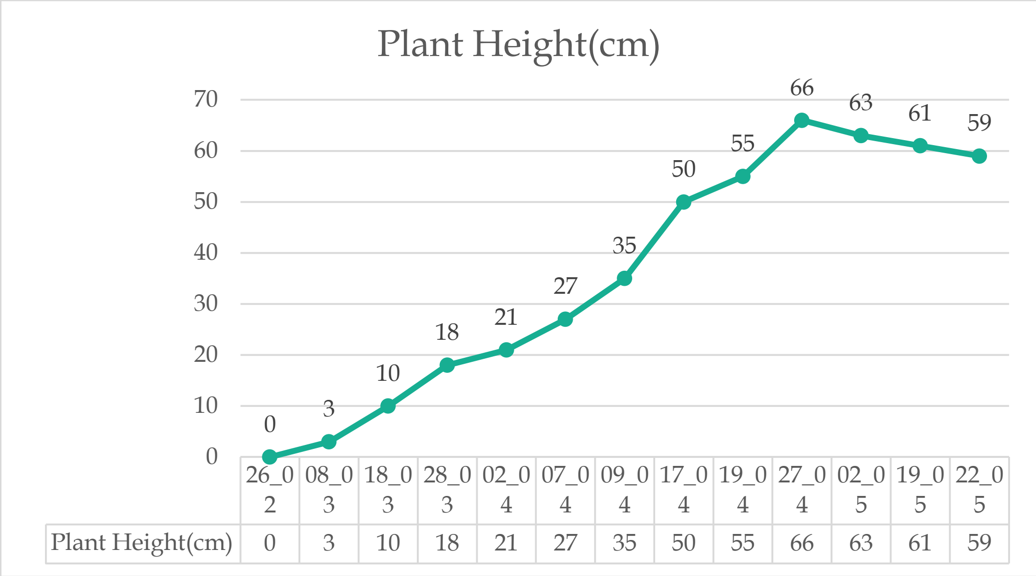

Figure 17:

1.1 Satellite Data Source

The **Copernicus Open Access Hub** (European Space Agency – ESA) was used as the platform to download free satellite imagery. **Sentinel-2** images were selected, specifically the **Level-2A** product (atmospherically and radiometrically corrected), covering the barley growing period from February to May 2026.

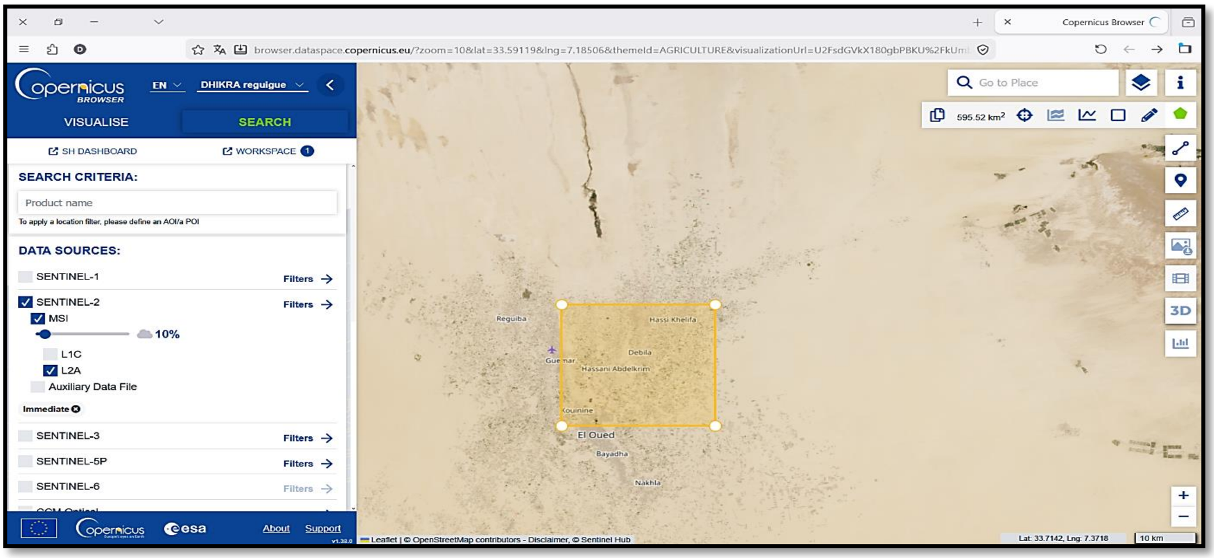

Figure 18: Copernicus

1.2 Processing Software

The following software packages were used for image processing and analysis:

- **QGIS software (version 3.44 'Solothurm):** An open-source geographic information system (GIS) used to compute the Normalized Difference Vegetation Index (NDVI) from satellite images.
- **Microsoft Excel:** Used to plot the NDVI time-series curve and interpret it over time.

1.3 Spatial Area of Interest (Satellite)

The Area of Interest (AOI) was defined as the **experimental barley field in the Debila area** (using its known dimensions or the previously recorded 10×10 m ground pixel coordinates). The GPS coordinates of the pixel were used to accurately locate the field on the satellite images.

2. Method

2.1 Downloading Satellite Images from Copernicus

The Copernicus Open Access Hub (or Copernicus Data Space Ecosystem) was accessed after creating a user account. For the Debila study area (southern Algeria), where the sowing date was February 26, 2026, the following twelve search criteria were systematically applied:

- **Mission:** Sentinel-2
- **Satellite Platform:** Sentinel-2A and Sentinel-2B
- **Processing Level:** Level 2A
- **Collection:** S2L2A
- **Sensing Date:** from February 26, 2026 (sowing date) up to the 12th week after sowing
- **Ingestion Date:** no specific constraint
- **Cloud Cover:** less than 10%
- **Orbit Number:** not predefined
- **Relative Orbit Number:** not predefined
- **Tile Number:** selected based on the Debila area coordinates (using the field coordinates or by selecting the area on the map)
- **Product Type:** S2MSI2A

- **Filename:** no specific constraint

Images covering each week of the study period were downloaded.

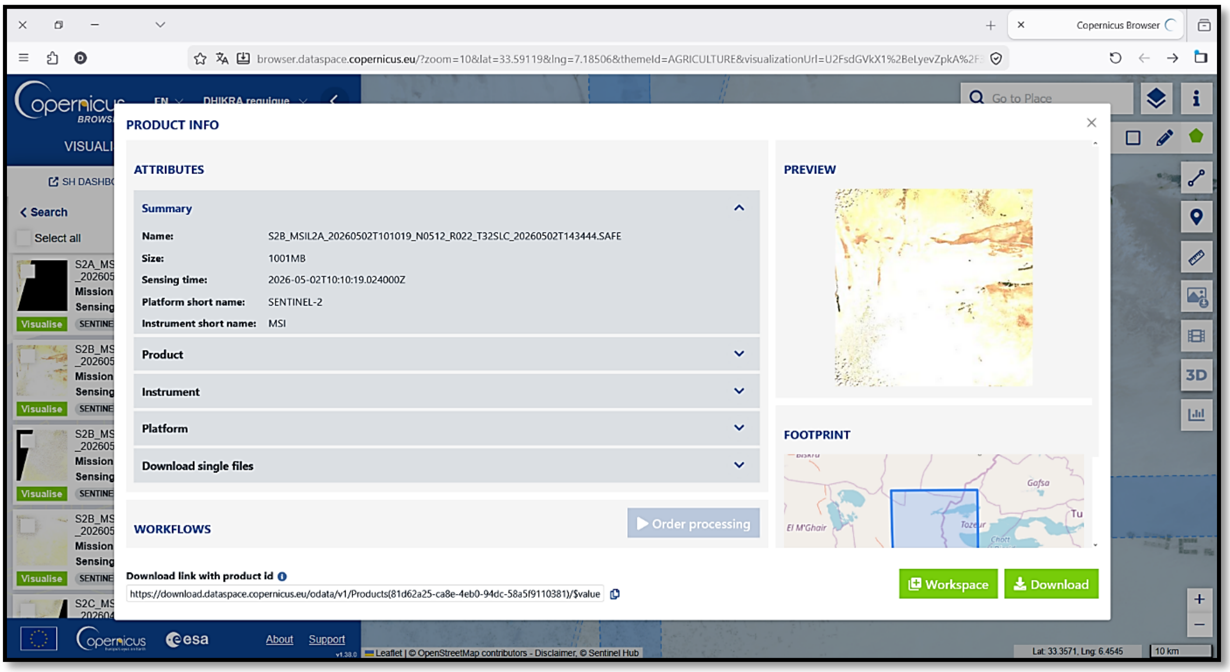

Figure 19: Downloading Satellite Images from Copernicus

2.2 NDVI Calculation Using QGIS

Each downloaded satellite image was opened in **QGIS**. The NDVI was computed using the **Raster Calculator** according to the following equation:

$$NDVI = \frac{(NIR-Red)}{(NIR+Red)} \ldots \ldots \ldots \ldots \ldots .4 \text{ (Mahmood \& Al-Rawe, 2023)}$$

where:

- **NIR:** Near-infrared band (Band 8 for Sentinel-2)
- **Red:** Red band (Band 4 for Sentinel-2)

The equation was applied to each image individually, producing new raster layers containing NDVI values.

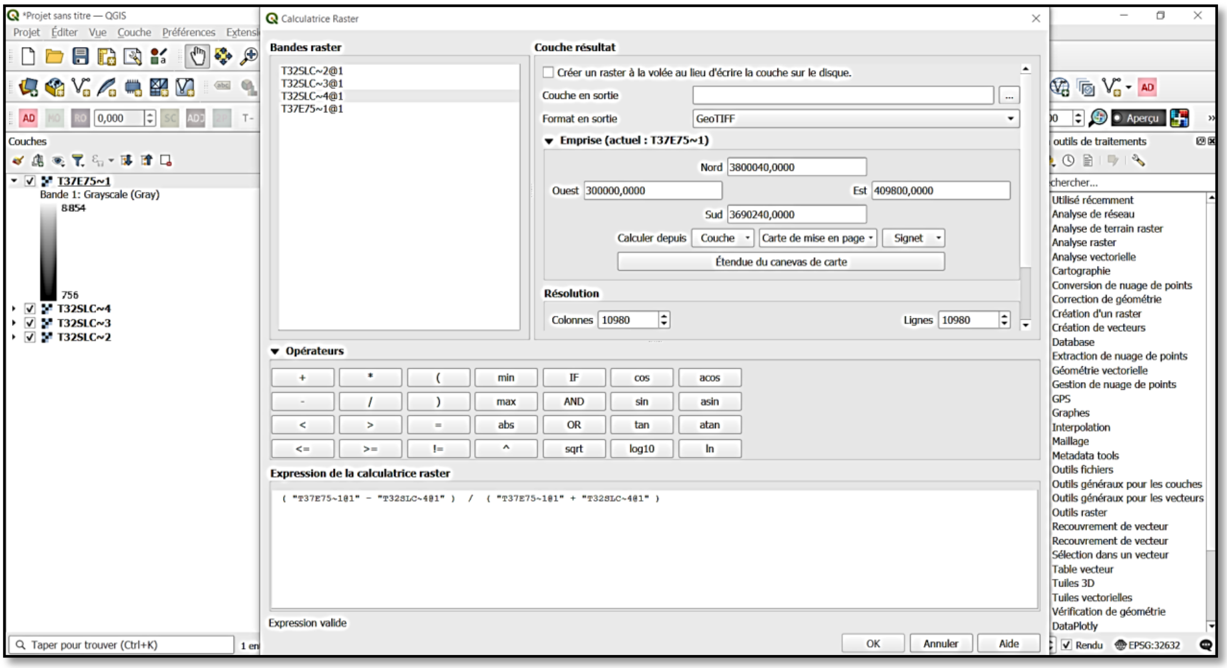

Figure 20: NDVI Calculation Using QGIS

2.3 Extracting NDVI Values for the Barley Field (10×10 m pixel)

Using the **Point Sampling Tool** or **Zonal Statistics** in QGIS, and based on the pre-defined pixel coordinates (10 m × 10 m), NDVI values were extracted for the same dates as the field measurements (each week of the study period). These values were recorded in a dedicated table containing: week number after sowing, and the corresponding NDVI value.

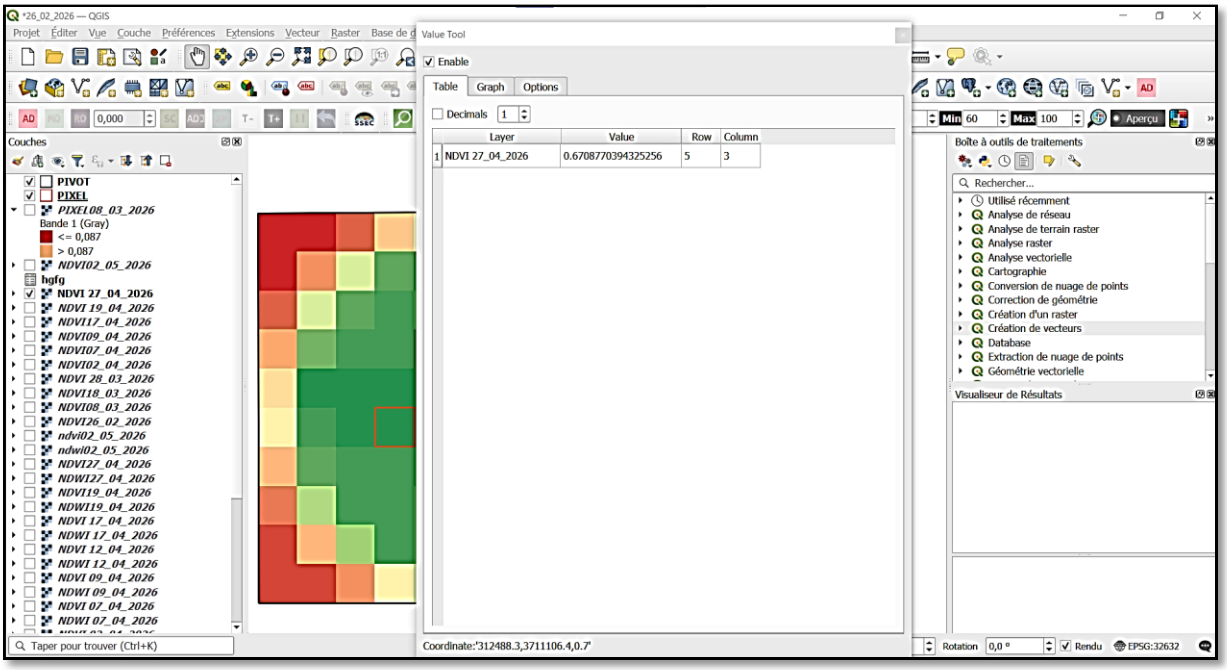

Figure 21: NDVI Values

2.4 Plotting the NDVI Curve Using Excel

The extracted weekly NDVI values were entered into an **Excel** worksheet with two columns:

- **Column 1 (X-axis – abscissa):** Weeks after sowing (1 to 12)
- **Column 2 (Y-axis – ordinate):** Corresponding NDVI values

A **"Line with Markers"** chart type was selected. The X-axis was set to weeks after sowing, and the Y-axis to NDVI values. After generating the chart, the following labels were added:

- Chart title: **"NDVI Curve of Barley Under Center-Pivot Irrigation"**
- X-axis title: **"Week After Sowing (week)"**
- Y-axis title: **"NDVI Value"**

This produced a curve illustrating the development of green biomass of barley as observed by satellite during the growing season.

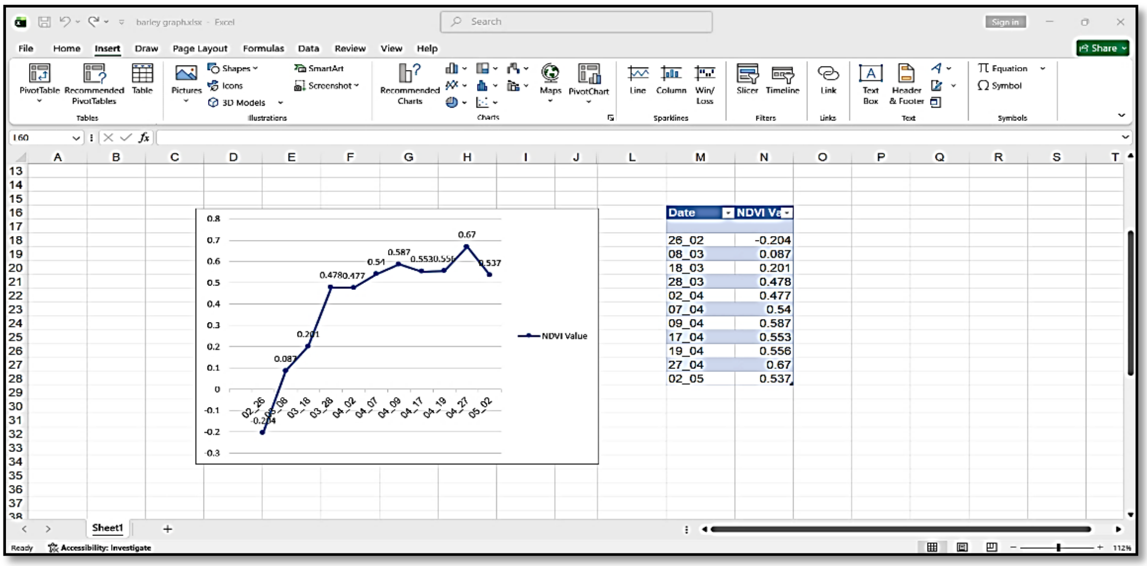

Figure 22: Excel

Date	Plant Height(cm)	NDVI
26_02	0	0
08_03	3	0.087
18_03	10	0.201
28_03	18	0.478
02_04	21	0.477
07_04	27	0.54
09_04	35	0.587
17_04	50	0.553
19_04	55	0.556
27_04	66	0.67
02_05	63	0.537
19_05	61	0.524
22_05	59	0.507

Table 11: NDVI and Plant Height (cm) by Week

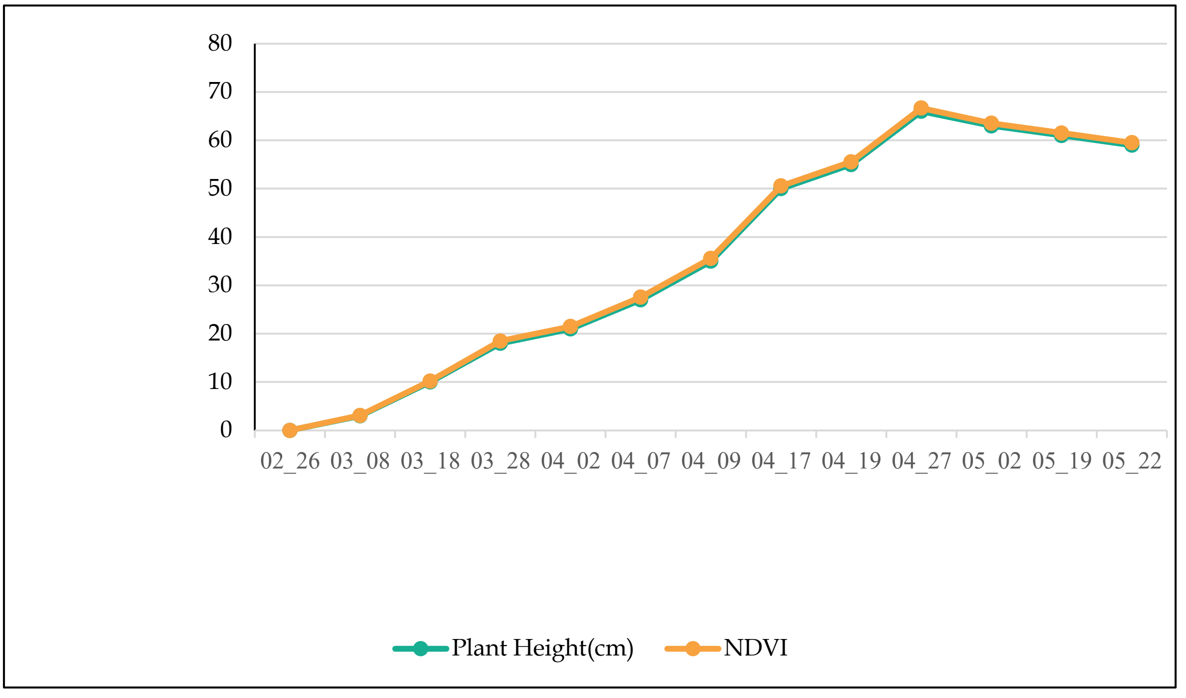

Figure 23:Temporal Curves of Weekly NDVI Values and Barley Plant Height (cm)

3. Results:

Table (11) shows both the weekly change in the average height of barley plants and the change in NDVI values over the same period. Plant height exhibited a gradual increase from a minimum value of 3 cm in the first week to a maximum of 65 cm by week ten, with a marked acceleration in growth between weeks four and seven. NDVI values started low (0.087) in the first week, then increased progressively to reach their peak (0.67) in the ninth week, and subsequently declined by week twelve, reflecting the onset of physiological maturity and reduced photosynthetic activity.

To quantitatively assess the relationship between the two indicators, a scatter plot was generated relating plant height to NDVI values, and a second-degree polynomial trendline was added using Microsoft Excel. The plot revealed a coefficient of determination (R^2) of 0.9051 (for example, the value is typically higher than that of the linear model because the curve captures the nonlinear trend), indicating that 90% of the variability in NDVI could be explained by plant height according to the polynomial model. Since the relationship is nonlinear, Pearson's correlation coefficient (which assumes linearity) was not used; instead, the coefficient of determination R^2 was relied upon to confirm the strong nonlinear relationship between barley vertical growth and NDVI values.

These results are consistent with the actual barley measurement table, where the plant reaches its maximum height between weeks nine and ten, while NDVI peaks at week nine and then declines, confirming that the spectral index accurately reflects the actual physiological status of the plant.

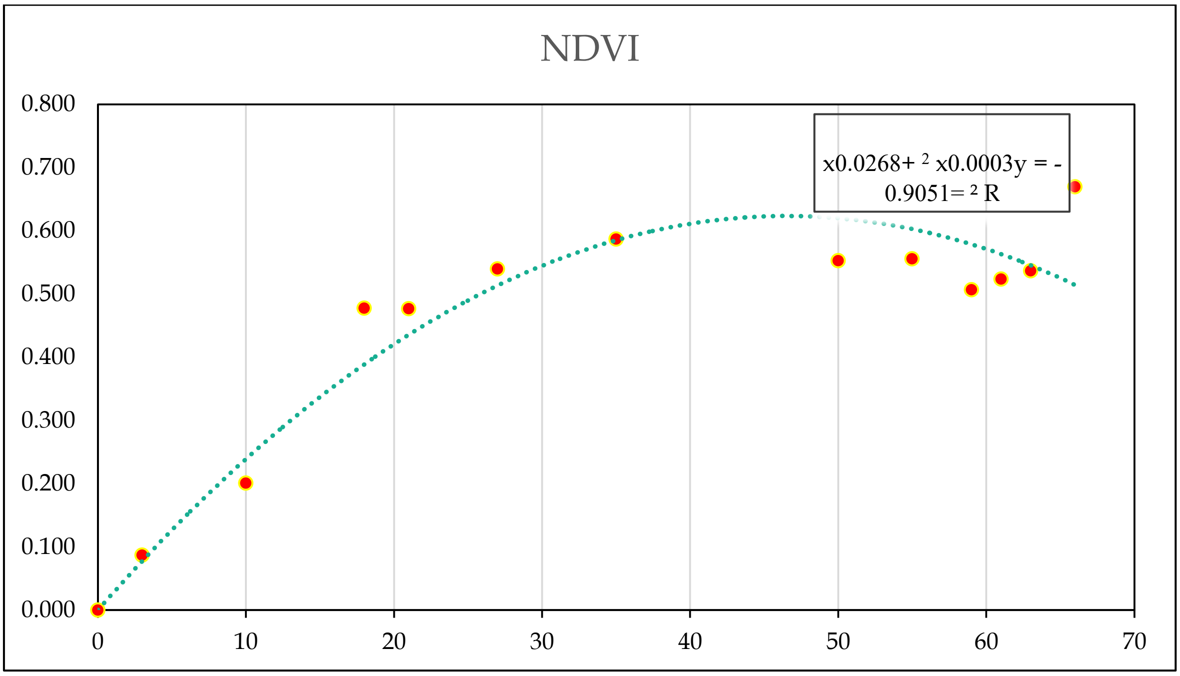

Figure 24:Scatter Plot with Second-Degree Polynomial Trendline: NDVI vs. Plant Height

The NDVI **map** shows very low values (near zero) on the first day after planting due to the lack of vegetation cover. By week three, a clear increase is observed, indicating the beginning of active vegetative growth. Values gradually rise to a peak of 0.67 by week nine, when the crop reaches maximum greenness. Subsequently, by week twelve, the map reveals a distinct decline in NDVI, reflecting physiological maturity, leaf senescence, and reduced photosynthetic activity.

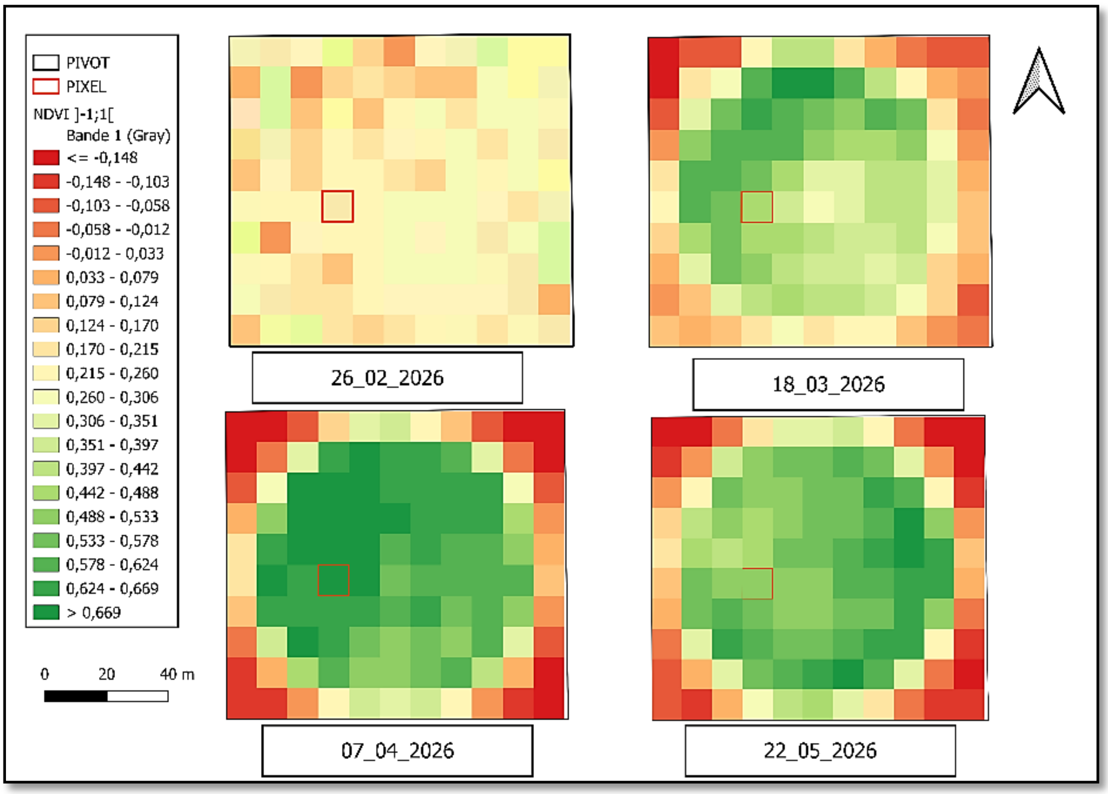

Figure 25: NDVI Map of Barley Vegetation Cover

4. Discussion:

The results of this study reveal a strong agreement between the NDVI index and the vertical growth of barley plants, with a coefficient of determination (R^2) of 0.9051 when using a second-degree polynomial model. This high level of explained variance indicates that 90% of the variability in NDVI values can be accounted for by changes in plant height, reflecting the ability of the spectral index to track vegetative growth with high accuracy. The polynomial model is more appropriate than the linear model for describing this relationship because the plant's physiological response is not entirely linear; the plant goes through phases of rapid growth followed by slower growth, which the polynomial curve captures more effectively.

Synchrony Between NDVI and Plant Height in Early Stages

The simultaneous upward trend of both NDVI and plant height during the first six weeks (weeks 1–7) reflects a normal physiological response after sowing. The rapid increase in NDVI coincides with the onset of accelerated vertical growth and is associated with increased chlorophyll content in young leaves and photosynthetic efficiency. At this stage, plants invest their energy in producing green biomass, which is clearly reflected in both indicators.

NDVI Peaks Before Maximum Plant Height

It is notable that NDVI reaches its peak (0.67) at week nine, while the plant attains its maximum height (65 cm) at week ten. This temporal lag can be explained by the fact that the NDVI index is primarily sensitive to green, photosynthetically active biomass rather than to purely mechanical stem elongation. In the pre-maturity stage, the upper leaves achieve their maximum photosynthetic efficiency, but the plant may continue slight vegetative elongation while chlorophyll activity gradually declines in the lower leaves. This behavior explains why plant height continues to increase while NDVI stabilises or decreases slightly.

Decline in NDVI with Physiological Maturity

The noticeable decline in NDVI values by week twelve reflects the onset of physiological maturity, where lower leaves progressively lose their chlorophyll content, leading to senescence and reduced photosynthetic capacity. This process is normal toward the end of the barley life cycle and is fully consistent with the actual measurement table, which shows that plant height stabilises after week ten. This decline confirms that changes in NDVI are not a measurement artifact but a genuine physiological condition.

Accuracy of NDVI Maps in Tracking Seasonal Growth

The presented NDVI maps confirm the same temporal trends: very low values near zero on the first day after planting (absence of vegetation cover), a clear increase by week three (beginning of active vegetative growth), a peak of 0.67 by week nine (maximum greenness), and a distinct decline by week twelve (maturity and senescence). This consistency between numerical analysis and mapping reinforces the reliability of the index.

CHAPTER II Case Study (OUED RIGH)

1.1Study Area:

The Oued Righ Region (valley)

Located in the northeastern part of the Algerian Sahara, the Oued Righ region extends linearly from south to north over a distance of approximately 170 km, between latitudes 32.54° N and 34.9° N.

From a climatic perspective, average temperatures exceed 20°C for more than six months of the year, and annual rainfall does not reach 100 mm, despite the region being situated only 300 km from the coast. Oued Righ lies at the center of a vast artesian basin, composed of a multi-layered aquifer system. The shallowest of these aquifers has enabled the reclamation of arid lands and the development of oasis agriculture for several centuries.

Today, the Oued Righ region is divided into three major date palm agglomerations: El Meghaïer in the north, Jamaa in the center, and Touggourt in the south. Covering an area exceeding 20,000 hectares, these palm groves contain over 2 million date palms, making them the largest concentration of palm trees in the entire Sahara Desert. Administratively, Touggourt is a district (daïra) within the province (wilaya) of Ouargla, while Jamaa and El Meghaïer are districts belonging to the province of El Oued. (Djouadi Bettiche, 2011)

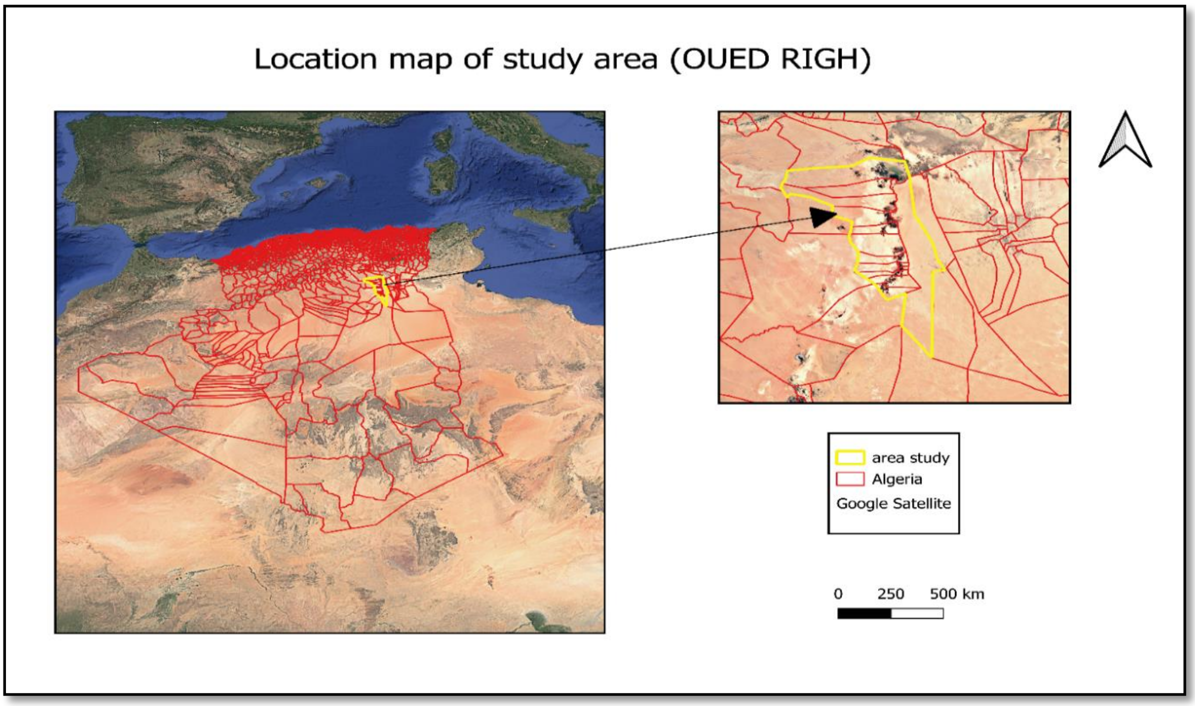

Figure 26: location map of study area Oued Righ

1.2 Satellite Data (Sentinel-2 Dataset)

This study relied on multi-temporal satellite imagery from the Sentinel-2 platform, owing to its integrated spectral and spatial capabilities. (Kovács et al., 2026)

- **Launch year**: 2015 (Sentinel-2A)
- **Swath width**: 290 km
- **Spectral bands**: 13
- **Spatial resolution:**
  - o Four visible and near-infrared (NIR) bands at 10 m:
    - B2 (Blue, 490 nm)
    - B3 (Green, 560 nm)
    - B4 (Red, 665 nm)
    - B8 (NIR, 842 nm)
  - o Six red-edge and shortwave infrared (SWIR) bands at 20 m:
    - B5 (Red Edge 1, 705 nm)
    - B6 (Red Edge 2, 740 nm)
    - B7 (Red Edge 3, 783 nm)
    - B8a (NIR narrow, 865 nm)
    - B11 (SWIR 1, 1610 nm)
    - B12 (SWIR 2, 2190 nm)
  - o Three atmospheric bands for correction at 60 m:
    - B1 (Coastal aerosol, 443 nm)
    - B9 (Water vapour, 940 nm)
    - B10 (Cirrus, 1375 nm)

Offers high revisit frequency and superior red-edge sensitivity, making it highly suitable for vegetation and soil moisture monitoring.

The study monitored vegetation cover in the region throughout the period from 2016 to 2026, employing remote sensing techniques and Geographic Information Systems (GIS) to track and analyze land use and land cover changes. A total of ten satellite images were processed over consecutive time intervals (2016, 2017, 2018, 2019, 2020, 2021, 2022, 2023, 2024, 2025, and2026). Various spatial analysis tools and methods available within GIS technology were utilized to identify and assess the spatiotemporal dynamics of vegetation growth and development across the study area.

3. Calculation and Analysis of the NDVI Spectral Index:

The study relied on the analysis of a spectral index derived from Sentinel-2 images, namely the Normalized Difference Vegetation Index (NDVI), with the aim of assessing and estimating the density and vitality of vegetation. This index is based on the difference between the reflectance in the near-infrared (NIR) and the red (RED) bands, and is calculated according to the following equation:

$$NDVI = \frac{NIR - RED}{NIR + RED} \dots\dots\dots\dots\dots\dots. (04)(\text{Mahmood \& Al-Rawe, 2023})$$

High values of this index indicate the presence of dense and active vegetation, whereas low values indicate sparse or degraded vegetation.

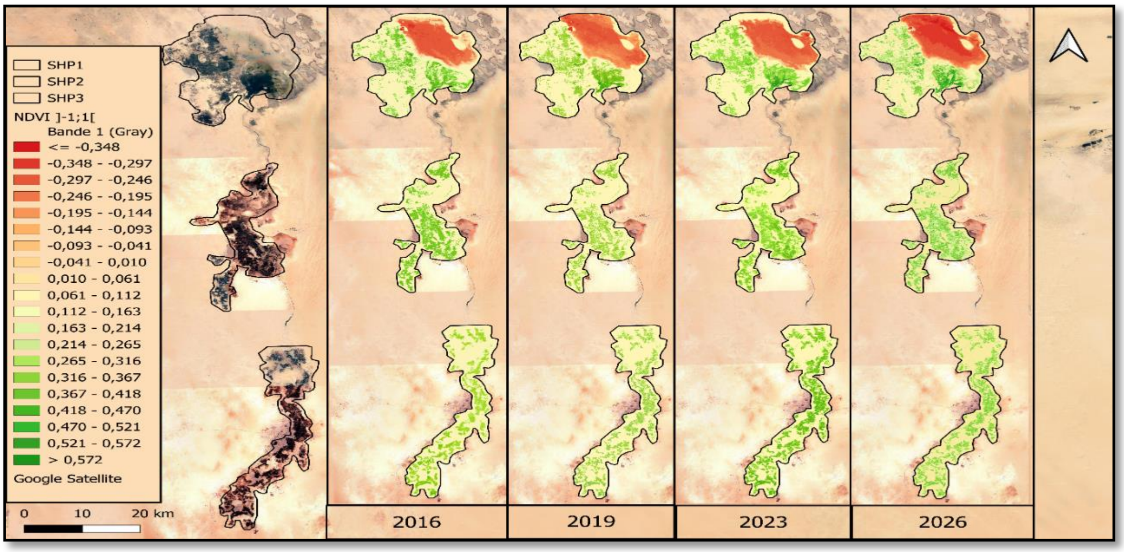

Figure 27: NDVI Map of the Oued Righ Region(2026–2016)

4. Results:

4.1 NDVI Class Distribution (2016–2026)

The analysis of pixel frequency across seven NDVI intervals revealed distinct temporal patterns over the 11-year study period (2016–2026). The class intervals and their ecological interpretations are summarized below:

- **Class 1 (-0.6 to -0.4)**: Water bodies, very wet soil, dense shadows.
- **Class 2 (-0.4 to -0.2)**: Moist soil, non-vegetated surfaces.
- **Class 3 (-0.2 to 0)**: Bare soil, dead or extremely sparse vegetation.

- **Class 4 (0 to 0.2)**: Bare soil or sparse, weak vegetation.
- **Class 5 (0.2 to 0.4)**: Moderate vegetation (grasslands, crops).
- **Class 6 (0.4 to 0.6)**: Dense, healthy vegetation (forests, vigorous crops).
- **Class 7 (0.6 to 0.8)**: Very dense vegetation (rainforests, extremely lush crops).

Table 12: Pixel Count Distribution Across NDVI Classes (2016–2026)

NDVI	]-0.6;-0.4]	]-0.4;-0.2]	]-0.2;0]	]0;0.2]	]0.2;0.4]	]0.4;0,6]	]0.6;0.8]
2026	529	1128659	215109	5903159	1960634	198540	2543
2025	41	962574	365139	5759117	2050385	268352	3565
2024	167732	1045018	4512606	2480976	1120247	82575	18
2023	21	690050	1927175	4942242	1644732	187235	17718
2022	107	686	3551720	5113667	684079	58276	638
2021	31	251	2143853	6146789	1106443	11405	401
2020	489	397923	3418829	3516698	1477361	594079	3794
2019	180	411001	879370	5575961	1742802	698520	101339
2018	137181	793145	2481906	5070154	881357	45430	0
2017	362	731671	2520358	3746230	1807638	582948	19966
2016	19305	1113452	1617057	5323997	1270144	64896	322

4.1.1 High NDVI Classes (NDVI > 0.4) – Healthy, Dense Vegetation

- **Class 0.4–0.6**: Pixel counts ranged from approximately 0.58 million (2017: 582,948) to 2.05 million (2025: 2,050,385). A progressive increase was observed from 2020 (1.48 million) to 2025, followed by a modest decline in 2026 (1.96 million).
- **Class 0.6–0.8**: Values were very low or zero in most years (e.g., 2018: 0; 2021: 401; 2020: 3,794; 2023: 17,718; 2025: 3,565). The highest recorded value occurred in 2019 (101,339), followed by 2017 (19,966) and 2023 (17,718). In recent years (2025, 2026), counts remained far below the 2019 peak, indicating that very dense vegetation is both rare and highly variable.

4.1.2 Moderate NDVI Class (0.2–0.4) – Moderate Vegetation

- This class dominated in several years. Pixel counts were: 2016 = 5.32M, 2017 = 3.75M, 2018 = 5.07M, 2019 = 5.58M, 2020 = 3.52M, 2021 = 6.15M (peak), 2022 = 5.11M, 2023 = 4.94M, 2024 = 2.48M (sharp drop), 2025 = 5.76M, 2026 = 5.90M. A marked decline was observed in 2024, followed by recovery in 2025–2026.

4.1.3 Low NDVI Class (0–0.2) – Bare Soil / Weak Vegetation

- Pixel counts ranged from 3.55M (2022) to 6.15M (2021). The highest count was recorded in 2021 (6.15M). This class contained the largest number of pixels in most years, except when the 0.2–0.4 class occasionally surpassed it, suggesting that the study area is frequently dominated by bare soil or very sparse vegetation.

4.1.4 Negative NDVI Classes (NDVI < 0)

- These classes increased markedly in 2024 (class -0.2 to 0: 4.51M; class -0.4 to -0.2: 1.045M; class -0.6 to -0.4: 0.168M), as well as in 2018 (2.48M) and 2016 (1.62M). High values in 2024 indicated widespread non-vegetated conditions (e.g., recently ploughed fields or wetlands).

4.2 Temporal Trajectory of NDVI Classes

When plotted over time, the following trends were observed:

- **Class 0–0.2**: Peaked in 2021 (6.15M), dropped sharply to 2.48M in 2024, then rose again to 5.90M in 2026 – highly variable.
- **Class 0.2–0.4**: Fluctuated widely, with a notable decline in 2024 followed by recovery.
- **Class 0.4–0.6**: Showed a generally increasing trend from 2019 (698,520) to 2025 (2,050,385), then a slight decrease in 2026.
- **Class >0.6**: Exhibited a distinct peak in 2019 (101,339), then declined, followed by a modest rise in 2023 (17,718) and another decrease thereafter.

A key observation was the unusual increase in negative NDVI classes and the 0–0.2 class in 2024, accompanied by a sharp decline in the 0.2–0.4 class.

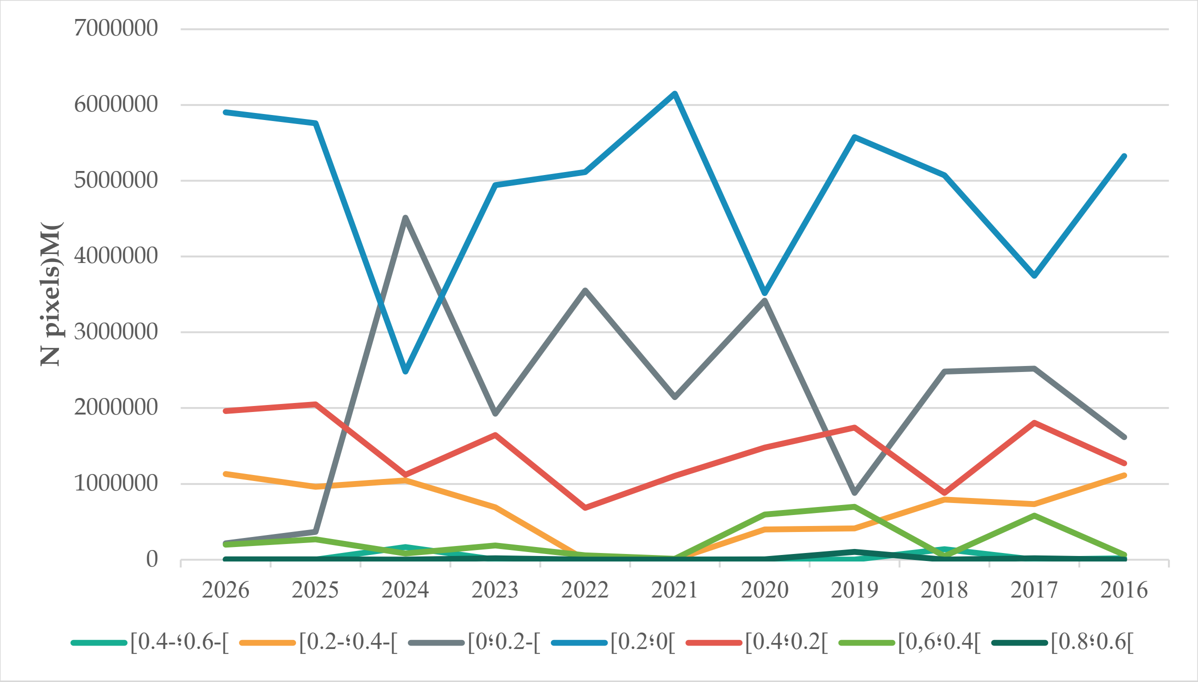

Figur 28:Temporal Curves of NDVI Values and Pixel Count Distribution–2016) (2026

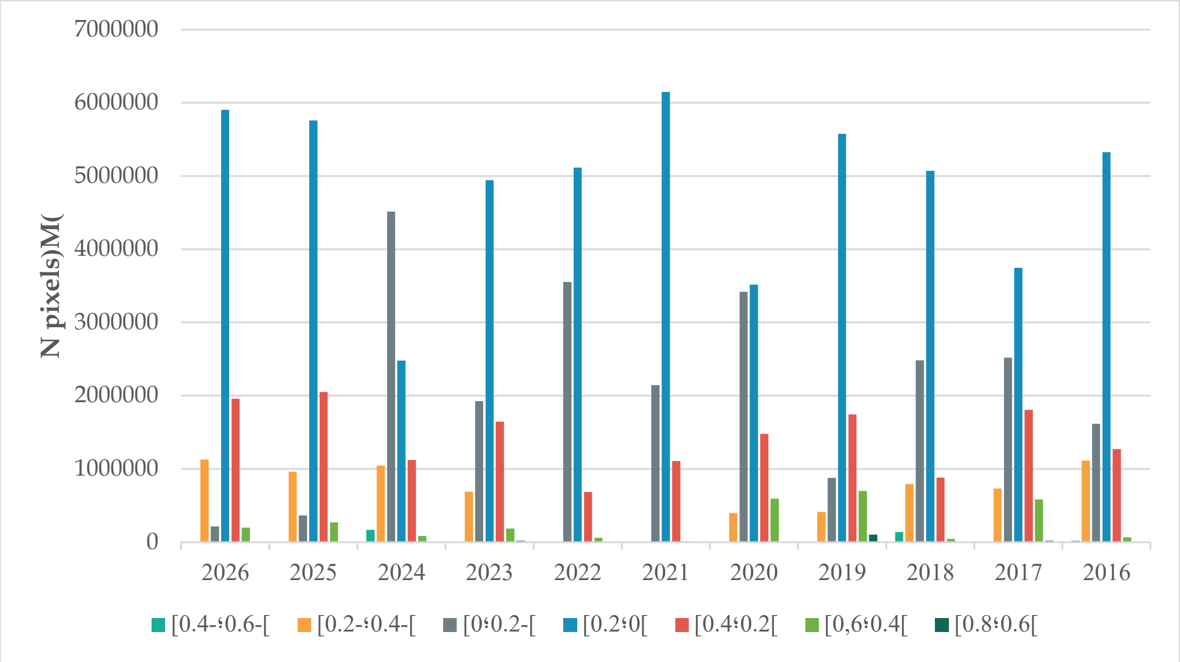

Figure 29: Bar Chart of Temporal Changes in NDVI Values and Pixel Counts (2026–2016)

5. Discussion

5.1 Relationship Between Climatic Variability and NDVI Distribution

The temporal patterns of NDVI class distribution were compared with available climatic data (precipitation) for the Oued Righ region. A noticeable agreement emerged between the trajectory of vegetation cover and dry/wet fluctuations.

In 2016, which recorded approximately 35 mm of rainfall (Tutiempo, 2016) – a moderate value in an arid context – the NDVI distribution showed a clear presence of higher spectral classes (e.g., 0.4–0.6 and 0.6–0.8), though not the highest of the decade. This suggests that the region began the decade with some carry-over soil moisture from previous years, or that moderate rainfall was sufficient to sustain reasonable vegetation cover in a sensitive oasis system.

5.2 Impact of the Prolonged Drought Period (2017–2025)

During the extended drought from 2017 to 2025, characterized by a progressive rainfall deficit and, in many years, severe water scarcity, the NDVI distribution revealed a gradual structural shift. Higher classes progressively narrowed (or disappeared in the driest years), while lower classes (especially -0.2–0.0 and -0.4—0.2) expanded steadily, reflecting bare soil or very sparse vegetation. This trend is physiologically coherent: extended drought leads to surface soil desiccation, death of annual plants, and reduced vigour of perennial species (e.g., date palms), which is captured by NDVI values dropping below 0.2 over extensive areas.

5.3 Vegetation Recovery Following the 2026 Extreme Rainfall Event

In 2026, which witnessed exceptionally heavy rainfall and unprecedented flooding in the region, the NDVI distribution showed a sharp and marked recovery of the higher classes (0.4–0.8), possibly the largest area recorded over the ten-year period. This rapid recovery confirms that the Oued Righ ecosystem retains a capacity for temporary resilience when water becomes available: perennial and seasonal plants respond with a swift increase in green biomass and photosynthetic activity. It also demonstrates the high sensitivity of NDVI to short-term moisture changes, making it a suitable indicator for monitoring vegetation recovery after climatic shocks.

5.4 Non-Instantaneous Nature of the NDVI–Precipitation Relationship

It is worth noting that 2016 was not necessarily the wettest year (compared to 2026, for example), yet the NDVI distribution still showed a good presence of high classes. This implies that the relationship between precipitation and NDVI is not purely instantaneous; it is also modulated by soil moisture memory, temperature, wind, and human intervention.

5.5 Overall Consistency and Utility of NDVI as a Monitoring Tool

Overall, the consistency between the extended drought sequence (2017–2025) and the contraction of high NDVI classes, together with the link between the 2026 heavy rainfall and the recovery of those classes, strongly supports the conclusion that the NDVI index – especially when tracked as a frequency distribution across fine spectral classes – is a valid tool for monitoring drought history and environmental recovery in arid regions such as Oued Righ.

Conclusion

Integrating the Barley Field Study and the Oued Righ Region Study Proving the Effectiveness of GIS and Remote Sensing in Vegetation Cover Analysis and Monitoring

The findings obtained from these two chapters demonstrate that remote sensing techniques and Geographic Information Systems (GIS) constitute effective and reliable tools for monitoring, analysing, and assessing vegetation cover at different spatial and temporal scales.

In the first chapter (Barley field study), a very strong correlation was established between the NDVI index and the vertical growth of barley plants, with a coefficient of determination (R^2) of 0.9051 and a Pearson correlation coefficient (r) of 0.9513. The results showed that NDVI rises simultaneously with the acceleration of vegetative growth, peaks at week nine before the plant reaches its maximum height, and then begins to decline as the plant enters physiological maturity by week twelve. This consistency with the actual field measurements confirms the ability of NDVI to accurately reflect the real physiological status of the plant, making it a non-destructive, rapid alternative to conventional field measurements.

In the second chapter (Oued Righ region study), the frequency distribution of NDVI values across seven spectral classes over ten years (2016–2026) enabled the tracking of spatial and temporal dynamics of vegetation cover in a semi-arid desert environment. The results showed a clear agreement between the trajectory of vegetation area changes (expressed as pixel counts per class) and recorded rainfall. During the prolonged drought period (2017–2025), the higher classes (NDVI > 0.4) contracted while the lower classes (NDVI < 0.2) expanded steadily. In contrast, the exceptionally wet year 2026 exhibited a sharp recovery of the higher classes. This confirms the high sensitivity of NDVI to climatic variability and its capacity to monitor both drought and environmental recovery.

By integrating the results of both chapters, we can affirm that remote sensing and GIS prove their value as an integrated scientific methodology for studying vegetation cover at two levels:

1. **Detailed (field) level**: NDVI can be reliably used to track the growth of an individual crop (e.g., barley), determine its phenological stages, and identify the optimal harvest timing, with accuracy comparable to field measurements.
2. **Spatial (regional) level**: NDVI can be used to monitor spatial and temporal changes in vegetation cover over large areas and across multiple years, providing a practical alternative to costly ground surveys.

The ability to convert satellite imagery into digital maps and quantitative values (such as NDVI) and to analyse them statistically using GIS opens broad horizons for applications in precision agriculture, natural resource management, desertification monitoring, and assessment of climate change impacts on fragile ecosystems such as desert oases.

The study recommends the widespread adoption of these techniques by agricultural and environmental institutions, the conduct of future studies linking NDVI to other climatic and edaphic factors, and the increased use of frequency-based analysis (NDVI classes) rather than mean values alone, owing to its superior ability to detect structural shifts in vegetation cover.

References

References

1. Abdaoui, G. R., Tabet, A. A., Bouaicha, F., Bousmaha, A., & Bouchemal, S. (n.d.). *Sprawl, Specificity and Dynamics of Inter-Municipal Urban Agglomerations of the Souf Valley (South East Algeria): Using GIS Techniques*.

2. Avery, W. (2018). Remote Sensing via Satellite Imagery Analysis. In A. Wahbi, L. Heng, & G. Dercon, *Cosmic Ray Neutron Sensing: Estimation of Agricultural Crop Biomass Water Equivalent* (pp. 11–23). Springer International Publishing. https://doi.org/10.1007/978-3-319-69539-6_3

3. Benyamina, B., & Hanane, G. (2025). Multispectral Indices for Crop Water Stress Assessment and Precision Irrigation in Arid Agriculture: A Case Study from Béchar, Algeria. *International Journal of Computational and Experimental Science and Engineering*, *11*(3). https://doi.org/10.22399/ijcesen.3414

4. Boulaaras, H., & Bouregaa, T. (2024). Cereal yield forecasting in semi-arid region of Algeria using MODIS-NDVI. *Journal of Aridland Agriculture*, 7–14. https://doi.org/10.25081/jaa.2024.v10.8562

5. Kumawat, R. K., Tiwari, G., Ramakrishnan, R. S., Bhayal, D., Debnath, S., Thakur, S., & Bhayal, L. (2023a). Remote Sensing Related Tools and their Spectral Indices Applications for Crop Management in Precision Agriculture. *International Journal of Environment and Climate Change*, 171–188. https://doi.org/10.9734/ijecc/2023/v13i11665

6. Kumawat, R. K., Tiwari, G., Ramakrishnan, R. S., Bhayal, D., Debnath, S., Thakur, S., & Bhayal, L. (2023b). Remote Sensing Related Tools and their Spectral Indices Applications for Crop Management in Precision Agriculture. *International Journal of Environment and Climate Change*, 171–188. https://doi.org/10.9734/ijecc/2023/v13i11665

7. Mahmood, M. A., & Al-Rawe, M. K. (2023). Spatial analysis of vegetation using GIS and remote sensing data. *IOP Conference Series: Earth and Environmental Science*, *1129*(1), 012001. https://doi.org/10.1088/1755-1315/1129/1/012001

8. Mayouf, R., Mennani, A., Hanafi, M. T., & Bouali, N. (2025). Integrating Sentinel-1 Sar and Landsat 8 Optical Data for Crop Type Discrimination and Vegetation Monitoring in Arid Zones of Algeria. *Agricultural Science Digest - A Research Journal*, (Of). https://doi.org/10.18805/ag.DF-797

9. *mémoire_final_étude_de_la_salinité_des_sols_en_utilisant_les_SIG*. (n.d.).

10. Omia, E., Bae, H., Park, E., Kim, M. S., Baek, I., Kabenge, I., & Cho, B.-K. (2023). Remote Sensing in Field Crop Monitoring: A Comprehensive Review of Sensor Systems, Data Analyses and Recent Advances. *Remote Sensing*, *15*(2), 354. https://doi.org/10.3390/rs15020354

11. Omol-Lecturer, E. (2019). BIT 2307: GEOGRAPHICAL INFORMATION SYSTEMS. *GEOGRAPHICAL INFORMATION SYSTEMS*.

12. Sangeetha, C., Moond, V., Rajesh G. M., Damor, J. S., Pandey, S. K., Kumar, P., & Singh, B. (2024). Remote Sensing and Geographic Information Systems for Precision Agriculture: A Review. *International Journal of Environment and Climate Change*, *14*(2), 287–309. https://doi.org/10.9734/ijecc/2024/v14i23945

13. Sishodia, R. P., Ray, R. L., & Singh, S. K. (2020a). Applications of Remote Sensing in Precision Agriculture: A Review. *Remote Sensing*, *12*(19), 3136. https://doi.org/10.3390/rs12193136

14. Sishodia, R. P., Ray, R. L., & Singh, S. K. (2020b). Applications of Remote Sensing in Precision Agriculture: A Review. *Remote Sensing*, *12*(19), 3136. https://doi.org/10.3390/rs12193136

15. Soum, A., Ayache, A., & Zoubidi, M. (2025). Attitudes of Algerian agricultural engineers towards the challenges facing precision agriculture adoption in Algeria. *Brazilian Journal of Animal and Environmental Research*, *8*(1), e77198. https://doi.org/10.34188/bjaerv8n1-050

16. Tarek, M., Sabah, A., Reguia, K., Warda, C., & Ahmed, B. (2025). *THE IMPACT OF AGRICULTURAL DYNAMICS ON THE AQUIFER IN THE OUED SOUF REGION*. *15*(2).

17. Weiss, M., Jacob, F., & Duveiller, G. (2020). Remote sensing for agricultural applications: A meta-review. *Remote Sensing of Environment*, *236*, 111402. https://doi.org/10.1016/j.rse.2019.111402

18. Wilson, H., Govender, K., Ransom, C., Mokoatsi, B., & Lerm, E. R. (n.d.). *Geographic Information System (GIS) Educator Training Manual*.

19. Zaiz, I., & Boutoutaou, D. (2022). Irrigation Water Impact on Soil Properties in Arid Oued-Souf Region, Southeast Algeria. *GeoScience Engineering*, *68*(1), 70–81. https://doi.org/10.35180/gse-2022-0070

20. Zhang, J. (2025). The Principles, Applications, and Development Trends of GIS and Remote Sensing Technology in Precision Agriculture. *Theoretical and Natural Science*, *117*(1), 140–145. https://doi.org/10.54254/2753-8818/2025.LD25384

21. Zhang, S., Wang, X., Lin, H., Dong, Y., & Qiang, Z. (2025). A review of the application of UAV multispectral remote sensing technology in precision agriculture. *Smart Agricultural Technology*, *12*, 101406. https://doi.org/10.1016/j.atech.2025.101406

22. Tutiempo Network, S.L. (2016). *Climate Touggourt (Year 2016) - Climate data (605550)*. Retrieved from https://en.tutiempo.net/climate/2016/ws-605550.html

23. QGIS Project. (2026, March 6). Changelog for QGIS 4.0. Retrieved June 26, 2026, from https://changelog.qgis.org/en/version/4.0/

24. Djouadi Bettiche, F. (2011). *Recherche sur la dimension humaine dans la conservation des écosystèmes lacustres: Cas de Chott Merouane et Oued Khrouf, Daïra de Méghaier, Wilaya d'El Oued – Algérie* [Mémoire de magister, Université Mohamed Khider – Biskra].

25. Kovács, D. D., Musial, J., Bojanowski, J., Clarijs, D., de la Mar, J., & Zlinszky, A. (2026). Copernicus Data Space Ecosystem establishes public cloud processing for earth observation data. *Scientific Data*. https://doi.org/10.1038/s41597-026-06765-8